

**COMPUTATIONAL MODELING OF FLUID FLOW  
THROUGH OPEN CELLULAR STRUCTURES**

by

Lucas Attia

A thesis submitted to the Faculty of the University of Delaware in partial fulfillment  
of the requirements for the degree of Honors Degree in Major with Distinction

Spring 2021


© 2021 Lucas Attia

All Rights Reserved

**COMPUTATIONAL MODELING OF FLUID FLOW  
THROUGH OPEN CELLULAR STRUCTURES**


by

Lucas Attia

Approved:  \_\_\_\_\_

Catherine A. Fromen, PhD

Professor in charge of thesis on behalf of the Advisory Committee

Approved:  \_\_\_\_\_

Dionisios G. Vlachos, PhD

Committee member from the Department of Chemical and Biomolecular  
Engineering

Approved:  \_\_\_\_\_

X. Lucas Lu, PhD

Committee member from the Board of Senior Thesis Readers

Approved: \_\_\_\_\_

Michael Chajes, Ph.D.

Dean, University Honors Program

## **ACKNOWLEDGMENTS**

I would like to acknowledge Dr. Catherine A. Fromen for her support and dedicated mentorship throughout this thesis project and my entire undergraduate research career. I am grateful for her belief and investment in me as both a scientist and person. This work would not have been possible without the mentorship of Ian Woodward as well as the friendship and support of the entire Fromen Research Group. Ian has always been a willing technical sparring partner and has challenged me to think in new, deep ways. Dr. Dion G. Vlachos, Dr. X. Lucas Lu, and Dr. Abhinav Malhotra have provided excellent technical sounding boards and feedback throughout the thesis program, and I appreciate their generosity in time and attention. I also would like to thank my family, particularly my parents for continuously imparting their guidance and wisdom. My brothers, Peter and Ben continue to set the bar high for their youngest brother, and they never stop helping me climb to their level. My partner, Michaela, has always supported my goals and aspirations, and she is always there to remind me to enjoy the process rather than just the destination. I am blessed with a wonderful support network of family, friends, peers, and colleagues, for which I am very grateful.

## TABLE OF CONTENTS

LIST OF TABLES .....	vi
LIST OF FIGURES.....	vii
ABSTRACT .....	ix
1 INTRODUCTION.....	1
1.1 Background and Motivation .....	1
1.2 Recent Advances in Designing, Modeling, and Optimizing Cellular Structures.....	2
1.2.1 Theoretical Pressure Drop Models .....	3
1.2.2 Computational Pressure Drop and Lattice Optimization.....	5
1.3 Novelty .....	6
1.4 Research Goal and Scope .....	6
1.4.1 Approach and Thesis Overview .....	7
1.4.1.1 Aim 1: CFD Modeling of Flow Phenomena through Individual Unit Cells .....	7
1.4.1.2 Aim 2: CFD Modeling of Pressure Drop across Cubic Unit Cells with Varied Geometry .....	9
1.4.1.3 Aim 3: Optimizing pressure drop over lattice length.....	10
2 METHODS .....	11
2.1 CAD for Unit Cells and Lattice Structures.....	11
2.1.1 Workflow to Create a Cubic Unit Cell .....	11
2.1.2 Workflow to Create a Kelvin Unit Cell.....	12
2.1.3 Surface Area Calculation.....	12
2.2 Computational Fluids Dynamics .....	12
2.2.1 Unit Cell Geometry and Meshing in SimScale .....	13
2.2.2 CFD Simulation Boundary Conditions .....	15
2.2.3 Turbulence Modeling, Numerical Conditions, and Convergence .....	16
2.2.3.1 Mesh Independence.....	18
2.2.4 Plot Generation and Statistical Analysis in OriginLab.....	20
3 RESULTS AND DISCUSSION .....	21

3.1	Flow Visualization through Single Unit Cell .....	21
3.1.1	Cubic Unit Cell.....	22
3.1.2	Kelvin Unit Cell .....	24
3.2	Cubic-based Lattice Pressure Drop vs. Window Size .....	27
3.2.1	CFD Results .....	32
3.2.1.1	Constant Strut Radius Experiment .....	32
3.2.1.2	Constant Cell Length Experiment.....	35
3.2.2	Volume porosity as a pressure drop predictor .....	38
3.3	Lattice Negative Flow Decoupling.....	40
3.3.1	Cubic-based lattice .....	40
3.3.2	Kelvin-based lattice .....	44
4	CONCLUSIONS AND FUTURE PLANS .....	48
4.1	Conclusions .....	48
4.1.1	Flow Phenomena .....	48
4.2	Future Work .....	50
4.2.1	Optimization of pressure drop through lattice structures .....	50
4.2.1.1	Workflow for optimization of lattice design .....	50
	REFERENCES.....	54

## LIST OF TABLES

Table 1: Mesh quality metrics for CFD.....	15
Table 2: Unit cell geometries and flow conditions used for flow visualization through single unit cells.....	21
Table 3: Designs for Constant Cell Length and Strut Radius Designs.....	28
Table 4: RMSE values for model fits of CSR simulations under $Rewindow = 750$ .....	33
Table 5: RMSE values for model fits of CSR simulations under $V_{superficial} =$ $3.28 m/s$ .....	35
Table 6: RMSE values for model fits of CCL simulations. ....	37
Table 8: RMSE values for model fits of cubic lattice simulations.....	41
Table 9: RMSE values for model fits of Kelvin lattice simulations.....	45

## LIST OF FIGURES

Figure 1: A sample cubic unit cell generated from Fusion 360.....	8
Figure 3: (A) 2-Dimensional cross-sectional sketches used to create a cubic unit cell in Fusion 360. (B) X-Y sketch extrusion into 3-dimensions. (C) X-Z sketch extrusion into 3-dimensions. (D) Y-Z sketch extrusion into 3-dimensions. ....	11
Figure 4: Schematic showing meshing approaches for CFD simulations of a sample cubic lattice. (A) Shows the “void space” approach which meshes only the fluid domain. (B) Shows the “enclosure” approach which meshes the solid lattice inside of an enclosure.....	14
Figure 5: Simulation boundary conditions for CFD simulations. (A) Velocity inlet, (B) pressure outlet, (C) slip (no penetration) on open faces, (D) no slip on lattice-normal faces. ....	16
Figure 6: Sample residual convergence plot. Residuals for all properties reach a steady value below $10^{-4}$ . Slight oscillations in the range of $10^{-7}$ are tolerable. ....	17
Figure 7: Mesh independence study for cubic unit cells in the constant strut radius dataset. The pressure drop was determined to change under 0.1% for all unit cells. ....	18
Figure 8: Mesh independence study for Kelvin unit cells. The pressure drop was determined to change under 0.1% for all unit cells. ....	19
Figure 10: Flow visualization through a cubic unit cell. ....	23
Figure 11: Flow visualization through a Kelvin unit cell.....	25
Figure 12: Inlet face of the Kelvin unit cell. (A) Shows 2-dimensional projection of the inlet. (B) Highlights the pores through which flow focusing is observed. Blue ovals rest in the peripheral pores, while the red square fills the central pore.....	26
Figure 13: Volume Porosity for both the constant cell length and constant strut radius. For CCL, linear regression yields an $r^2_{\text{adjusted}} = 0.996$ . For CSR, linear regression yields an $r^2_{\text{adjusted}} = 0.952$ , and a logarithmic fit yields $r^2_{\text{adjusted}} = 0.986$ . ....	29
Figure 14: Volume-based surface area for CSR and CCL unit cell designs .....	31
Figure 15: Results from CFD simulations for the CSR dataset for a constant flow condition of $Re_{\text{window}} = 750$ . (A) Pressure drop across unit cell. (B) Pressure gradient across unit cell. ....	33

Figure 16: Results from CFD simulations for the CSR dataset for a constant flow condition of  $V_{superficial} = 3.28 \text{ m/s}$ . (A) Pressure drop across unit cell. (B) Pressure gradient across unit cell. ....34

Figure 17: Results from CFD simulations for the CSR dataset for a constant flow condition of  $Rewindow = 750$ . ....36

Figure 18: Results from CFD simulations for the CSR dataset for a constant flow condition of  $V_{superficial} = 3.28 \text{ m/s}$ . ....37

Figure 19: Pressure Drop vs Volume Porosity for the CSR and CCL experiments. For CCL  $Re = 750$ , linear regression yields an  $r^2_{adjusted} = 0.930$ . For CCL  $V = 3.28 \text{ m/s}$ , linear regression yields an  $r^2_{adjusted} = 0.972$ . For CSR  $Re = 750$ , linear regression yields an  $r^2_{adjusted} = 0.994$ . For CSR  $V = 3.28 \text{ m/s}$ , linear regression yields an  $r^2_{adjusted} = 0.985$ . ....39

Figure 20: Pressure drop for cubic lattices comprised of 1-5 unit cells in the axial direction. Model fits for the Darcy-Weisbach, Ergun Equation, and icPOCS models are included. ....41

Figure 21: Pressure drop decoupling after Nth unit cell for cubic lattice stack. ANOVA tested statistical difference between regression slopes and 0.  $N = 1$  p-value = 0.985.  $N = 2$  p-value = 0.515.  $N = 3$  p-value = 0.494. ....43

Figure 22: Pressure drop for Kelvin lattices comprised of 1-5 unit cells in the axial direction. Model fits for the Darcy-Weisbach, Ergun Equation, and Foam models are included. ....45

Figure 23: Flow decoupling after Nth unit cell for Kelvin lattice stack. ANOVA tested statistical difference between regression slopes and 0.  $N = 1$  p-value = 0.802.  $N = 2$  p-value = 0.828.  $N = 3$  p-value = 0.802. ....46

Figure 24: Schematic of optimization workflow .....53



## **ABSTRACT**

Porous media have long been used for chemical engineering applications that require mass and heat transfer, including catalysis and separations. Recently, additive manufacturing has allowed for the design of structured mesoscale porous structures, including open cellular structures and lattices, which can be used for applications ranging from biomedical implants to drug delivery to aeroelastic wing design. These structures have also garnered interest as a means to generate ordered porous media which can exhibit desired surface properties and imparts predictability. However, limited work has investigated the flow dynamics through these structures. This thesis leveraged computational fluid dynamics (CFD) as a tool to simulate fluid flow through open cellular structures. The flow phenomena through individual unit cells was investigated, and flow conditioning through unit cell pores was observed. The influence of unit cell geometry and flow conditions on pressure drop was also investigated for cubic unit cells. Theoretical model fits were evaluated, and it was found that the Darcy-Weisbach model may be a useful tool to evaluate pressure drop over individual unit cells. Pressure drop was shown to be decoupled for cubic unit cells under laminar flow in lattice structures, suggesting the feasibility of implementing optimization for the design of lattice structures with specific flow dynamics. Finally, a portable optimization workflow was developed to optimize lattice designs with a minimum pressure drop.

## Chapter 1

### INTRODUCTION

#### 1.1 Background and Motivation

Recent advancements in additive manufacturing techniques have allowed for the generation of a wide array of precise geometries on the mesoscale. A major development has included the generation of regular lattice structures, which is an architecture formed by repeating unit cells comprised of edges and faces, with struts connecting different faces.<sup>1,2</sup> These lattices have exhibited improved mechanical properties, including increased strength, energy absorption, and selective porosity, while minimizing weight, material utilized and production time<sup>1,2</sup> Due to these improved properties, lattice structured have been utilized in many applications, functioning as load-bearing structures, particle collections, filters, catalytic supports, and even as organ scaffolds.<sup>1,3</sup> Because their structures can be defined *a priori* and remain static, additively manufactured periodic structures, encompassing beam lattices, surface lattices, and arranged polyhedra, have emerged as a viable option for creating rationally designed, ordered packings. This is valuable for chromatography and separations processes, where the ability to generate an ordered bed facilitates numerical simulation and comparison between packing geometries. Furthermore, given their foam likeness, beam lattices can also be used as platforms for catalytic process intensification. The most commonly studied structures in this field are the cubic unit cell lattice, due it its simplicity in design and production, and the Kelvin cell lattice, which represents the idealization of the stochastic foam structures currently in use. The advantages of using these structures as porous media are that they are easily lent to systematic study and modification, and because they are able to achieve high surface areas with

low porosity and tortuosity, they result in lower pressure drop and energy loss than stochastic open cell foams. However, despite being widely utilized, the physical behavior of these structures is not always fully understood, leading to efficiency loss in some applications and limited commercial translation for other new applications.

Specifically, flow-related phenomena in lattice structures are poorly understood.<sup>3,4,5</sup> The relationship between lattice structure and pressure drop across a lattice is especially understudied and is vital for the application of lattice structures as pressure modulators, filters, microreactors, or particle collectors . Preliminary experimental work has been done on the pressure drop across lattice structure,<sup>3</sup> and some theoretical modeling has been performed to correlate pressure drop across related structures, open-cell foams.<sup>4</sup>

However, while there has been limited work validating theoretical models for pressure drop over cellular structures, little work has applied computational fluid dynamic (CFD) tools to simulate flow through these structures. CFD is a numerical analysis tool that allows for the precise computational of fluid transport properties (pressure, velocity, shear stress) over a discretized geometry. This tool has been widely used to investigate many flow phenomena. This project investigates theoretical and computational models relating to the flow behavior through lattice structures of different unit cell geometries, with particular attention paid to the pressure drop observed over the length of a unit cell. The goal of this project is to develop the fundamental understanding in order to develop a framework for the optimization and design of a lattice structure which would exhibit desired flow dynamics for various applications.

## **1.2 Recent Advances in Designing, Modeling, and Optimizing Cellular Structures**

While the literature in modeling fluid flow through cellular structures is relatively new, there have been recent advances that are relevant to the scope and novelty of this project.

### 1.2.1 Theoretical Pressure Drop Models

Klumpp *et. al* and Inayat *et. al* have derived theoretical, physics-based correlations that predict the pressure drop across lattices composed of idealized cubic periodic open cellular structures (icPOCS) and idealized foams, respectively.<sup>3,4</sup> Previously, Inayat *et. al* (2011) conducted similar experimentation and derivations for ideal foams with tetrakaidecahedra packing.<sup>6</sup> These theoretical models were then validated experimentally, with success over specific unit cell geometries and volume porosity ranges. However, while these theoretical correlations proved useful for specific geometries, the range of geometries and flow conditions over which they are applicable is not well understood.

Equation 1 below shows the icPOCS model, which is the state-of-the-art pressure drop model for cubic lattice structures. The model relies on the area and volume based porosities, the fluid velocity, and the volume-based specific surface area. The model's derivation does not provide guidance over what porosity or fluid velocity ranges the model can be applied.

Equation 1: icPOCS Model.  $\Delta P$  = pressure drop.  $\Delta L$  = axial length.  $\varepsilon_A$  = area related porosity.  $\varepsilon_V$  = volume related porosity.  $\rho_f$  = fluid density.  $u_{sf,0}$  = superficial fluid velocity.  $a_V$  = total volume-based specific surface area.

$$\frac{\Delta P}{\Delta L} = \left( \frac{\varepsilon_A}{1 - \varepsilon_A} \right) * \frac{1 - \varepsilon_V}{\varepsilon_V} * \frac{\rho_f * a_V}{\varepsilon_V^3} * u_{sf,0}^2$$

Equation 2 below shows the Foam model, which is the state-of-the-art pressure drop model for cubic lattice structures. The model relies on the volume based porosity, the fluid velocity, and the tortuosity, which is a metric of the circuitousness of a streamline's path through the porous media. The model's derivation does not provide guidance over what porosity or fluid velocity ranges the model can be applied.

Equation 2: Foam Model  $\tau$  = tortuosity.  $\eta_f$  = fluid viscosity.  $D_H$  = hydraulic diameter.  $\alpha = 32$ .  
 $\beta = \frac{1}{2}$ .

$$\frac{\Delta P}{\Delta L} = \alpha * \tau^2 \left( \frac{\eta_f}{\varepsilon_V * D_H} \right) * u_{sf,0} + \beta * \frac{\tau^3}{2} \left( \frac{\rho_f}{\varepsilon_V^2 * D_H} \right) * u_{sf,0}^2$$

Traditional pressure drop through pipe flow is correlated using the Darcy-Weisbach model, which is shown in Equation 3. This model relies on only the fluid viscosity, flow rate, and hydraulic diameter. This form of the Darcy-Weisbach model is valid under laminar flow conditions, and can be analytically derived from Navier-Stokes equations, which are described in greater detail in Chapter 2.

Equation 3: Darcy-Weisbach Model.  $Q$  = fluid flowrate.

$$\frac{\Delta P}{\Delta L} = \frac{128}{\pi} * \frac{\eta_f * Q}{D_H^4}$$

The Ergun Equation is a physics-based correlation that describes fluid flow through porous media. The model relies on the area and volume based porosities, the fluid velocity, and the volume-based specific surface area.

Equation 4: Ergun Equation.  $\alpha = 4.16$   $\beta = 0.292$ .

$$\frac{\Delta P}{\Delta L} = \alpha \left( \frac{\eta_f * a_V^2}{\varepsilon_V^3} \right) * u_{sf,0} + \beta \left( \frac{\rho_f * a_V}{\varepsilon_V^3} \right) * u_{sf,0}^2$$

For lattice structures on the meso-scale, it is not well understood how well each of these models predict pressure drop. A goal of this thesis is to evaluate these models under varied flow conditions for a range of unit cell and lattice geometries.

### 1.2.2 Computational Pressure Drop and Lattice Optimization

There have also been recent advances in using CFD to model these flow dynamics through lattice structures. Computational fluid dynamics (CFD) is a numerical analysis method that is employed to simulate fluid flow in various systems.<sup>8,9</sup> CFD solvers numerically solve the partial differential equations (PDEs) that describe fluid flow, the Navier-Stokes equations. The Navier-Stokes equations describe the first principles conservation of momentum of fluid flow through infinitesimally discretized control volumes. Singh *et. al* used CFD to model flow through cubic unit cells in order to predict the permeability of lattices used in biomedical bone implants.<sup>7</sup> These results are used to inform the design of scaffolds in bone implant designs. Additionally, Bracconi *et. al* coupled CFD results to experimental validation of pressure gradients across idealized foams.<sup>8</sup> This validation led to a revised Ergun-like correlation for pressure drop across foams. Finally, Das *et. al* used CFD and multi-physics simulations to investigate flow and heat transport through randomized foams.<sup>9</sup>

Additionally, there has been substantial work in applying optimization techniques towards unit cell and lattice structure design.<sup>10</sup> However, these approaches have primarily aimed to optimize designs for mechanical and heat transfer properties of lattices. For example, Wang *et. al* used topological optimization to optimize the mechanical stiffness of graded lattice structures and validated their designs using experimentally-printed structures.<sup>11</sup> Daicong *et. al* similarly used topological optimization to maximize lattice mechanical stiffness.<sup>12</sup> They also incorporated the strain gradient of lattice structures into their optimization workflow, leading to improved mechanical properties. Finally, Abate *et. al* similarly looked to optimize the mechanical properties of lattice structures, expanding to several unit cell types and incorporating mechanical finite element analysis (FEA) into the optimization framework.<sup>13</sup>

### **1.3 Novelty**

This project builds upon the body of literature in modeling and optimization of cellular structures. The substantial theoretical work previously done has been experimentally validated for limited geometries but have not yet been widely applied to different types of lattice geometries, including volume porosity ranges and unit cell types. This work directly connects the pressure drop correlations developed in literature to CFD numerical predictions to wide range of volume porosities for cubic unit cells and lattices, as well as for lattices made from Kelvin unit cells.

The proposed workflow and methods of global optimization presented in this work here are novel. To our knowledge, the first work that proposes using simulation-generated data as input into a model for optimizing pressure drop over lattices. Above, other work has proposed and implemented optimization models for mechanical and heat transport properties, but similar models have not yet been proposed or implemented for fluid transport properties, specifically for pressure drop.

### **1.4 Research Goal and Scope**

The goal of this work is to develop computational models for the flow behavior of air through lattice structures of repeating unit cells with various dimensions and geometries. Accepted theoretical models established in literature are applied to the geometries and flow conditions tested computationally. After flow behavior was characterized for different flow rates and lattice geometries, a global multi-objective optimization workflow is developed proposed for the optimization of pressure drop over lattice length while minimizing material surface area. While the workflow has not yet been implemented, we hope future researchers will be able to readily implement this portable workflow.

### **1.4.1 Approach and Thesis Overview**

This thesis is organized into 4 Chapters. In Chapter 2, the computational and numerical methods are described, with attention paid in particular to CAD and CFD use. The experimental design for CFD simulations is also described. In Chapter 3, the results of CFD simulations and model fitting are presented and discussed. This chapter is divided into three subsections, which correspond to the three specific aims which are presented below. In Chapter 4, the key conclusions are summarized and the optimization workflow that was developed is presented.

The three specific aims of this thesis are summarized in terms of their goal, objective, approach, and key conclusions in the sections below. In Aim 1, our goal was to establish a CFD workflow to simulate fluid flow through unit cells and develop a qualitative understanding of the flow phenomena. In Aim 2, our goal was to probe how unit cell geometry and flow conditions influence pressure drop and to evaluate the suitability of different theoretical pressure drop models. In Aim 3, our goal was to investigate how fluid flow couples between unit cells in lattice structures, with an eye towards leveraging these results to implement an optimization workflow that can optimize a lattice design.

#### **1.4.1.1 Aim 1: CFD Modeling of Flow Phenomena through Individual Unit Cells**

The qualitative flow phenomena of fluid flow through computer aided design (CAD)-generated unit cells were first characterized using CFD simulations. The geometries of these unit cells were selected to match the geometries of unit cells that have been experimentally-tested within the Fromen Research Group. Unit cell geometries were computationally generated using the CAD software Fusion 360 Version 2.0.10148, licensed by Autodesk Inc.<sup>14</sup> A sample unit cell was generated and is shown below in Figure 1.



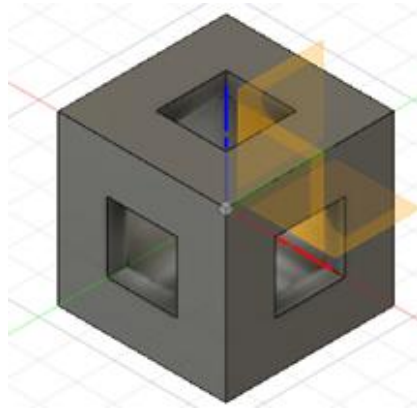


Figure 1: A sample cubic unit cell generated from Fusion 360.

Utilizing CFD simulations to investigate flow through unit cells offers distinct advantages over only experimentation. First, CFD allows for the solution of the flow parameter profiles throughout the lattice structure, rather than simply the inlet and outlet values. Additionally, CFD offers higher throughput than experimentation, which is important to simulate the wide variety of unit cell geometries of interest. For the sake of this project, we limited the unit cell geometries to cubic and Kelvin cells, but the platforms and simulations developed are readily applicable to other unit cell geometries. Flow through these structures was characterized using the open-sourced CFD software SimScale, developed by SimScale GmbH.<sup>15</sup> Metrics including the velocity counters, pressure drop profiles, turbulence, and flow streamlines were compared across unit cells geometries and flow conditions.

Overall, investigating the qualitative fluid flow phenomena trends show that flow profiles develop through unit cells in predictable ways. Velocity profiles show that fluid velocity in the axial direction experiences a “flow conditioning” effect, where velocity increases through the pores of unit cells. Additionally, transverse velocity is predictably induced as flow approaches struts. The predictability and control offered by fluid flow phenomena highlight the

promise order lattice structures offer to develop processes with highly controlled mass and heat transfer.

#### 1.4.1.2 Aim 2: CFD Modeling of Pressure Drop across Cubic Unit Cells with Varied Geometry

After flow was qualitatively characterized through individual unit cells, the effects of unit cell geometry on pressure drop were investigated. Two distinct experiments were developed. In the first, the strut size of cubic unit cells was kept constant, while the cell length was varied to achieve a desired set of window sizes. In the second, the cell length was kept constant, while the strut size was varied to achieve the same desired set of window sizes. For clarity, Equation 5 below shows the relationship between window size, strut radius, and cell length for a cubic unit cell.

Equation 5: Cubic unit cell geometric relationships.  $L_{window}$  = the length of one of the window dimensions.  $L_{cell}$  = the length of the unit cell.  $R_{strut}$  = the radius of a strut.

$$L_{window} = L_{cell} - 2 * R_{strut}$$

Two flow conditions were tested across these each of these sets of unit cell designs: (1) constant Reynolds number, as defined by the  $Re_{window}$  (shown below in Equation 6) and (2) constant superficial velocity at the unit cell inlet. Initial tests included cubic unit cell geometries with several strut and unit cell sizes over a range of air flowrates at standard pressure and viscosity.

Equation 6:  $Re_{window}$  as defined for a unit cell.  $\rho$  = fluid density.  $v$  = fluid velocity.  $\mu$  = fluid viscosity.  $D_H$  = hydraulic diameter.  $A$  = area of fluid inlet.  $P$  = perimeter of inlet.

$$Re_{window} = \frac{\rho v D_H}{\mu} \quad \text{Where: } D_H = \frac{4A}{P}$$

The relationship of individual unit cell geometry and flow conditions on pressure drop was investigated in-depth for cubic unit cells. It was observed that pressure drop was somewhat difficult to predict with the state-of-the-art theoretical correlations. Ultimately, the observed model fits do motivate the need for better a better physics-based correlation that is more adaptable to a diverse range of unit cell geometries and flow conditions. Volume porosity was shown to be a reasonably good linear predictor of pressure drop, particularly for porosity values above 0.9. While this does not replace the need for a robust correlation, it is useful as a predictive tool to leverage volume porosity as a pressure drop predictor.

#### **1.4.1.3 Aim 3: Optimizing pressure drop over lattice length**

Lattice structures have been optimized for certain mechanical applications, including load-bearing ability and mechanical stiffness. However, lattice structure optimization has not yet been attempted for flow-related applications. After CFD simulations were converged, we developed a global optimization workflow to obtain a multi-objective optimization . To do this, the coupling of flow through neighboring unit cells was examined for both cubic and Kelvin lattice assemblies. Flow was determined to be quantitatively decoupled between unit cells under specific flow conditions for both cubic and Kelvin unit cells. This allows for unit cells to be parameterized based on geometry alone (and not position) in a lattice assembly, which greatly simplifies the optimization of a lattice design. Once different unit cells are parameterized, machine learning techniques including univariate/multivariate regression, clustering, and principal component analysis (PCA) will be utilized to minimize or maximize desired flow variables, including particle impaction, pressure drop, or velocity drop. These optimized lattices would then be ready to be applied to the motivating applications previously mentioned, including utilization as pressure modulators or catalytic micro-reactors.

## Chapter 2

### METHODS

#### 2.1 CAD for Unit Cells and Lattice Structures

Computer-aided design (CAD) was used to design the unit cells and lattice structures studied in this project. The CAD software Fusion 360 Version 2.0.10148 , licensed by Autodesk Inc., was used to generate CAD geometries.

##### 2.1.1 Workflow to Create a Cubic Unit Cell

There are several design steps needed to create a cubic unit cell. First, a cross-sectional “sketch” is created, where the cylindrical struts are projected in 2-dimensional space as circles onto the corners of a square. This sketch is then repeated in the other 2 Cartesian planes. The 2-dimensional struts are then extruded into 3 dimensions to create a unit cell. The radius of the struts and the length of the cell are parameterized in Fusion 360 as mutable parameters such that cubic unit cells of varying dimensions can be created from the same workflow. Figure 3, below, shows the 2-dimensional sketches in each of the Cartesian planes, X-Y, X-Z, and Y-Z.

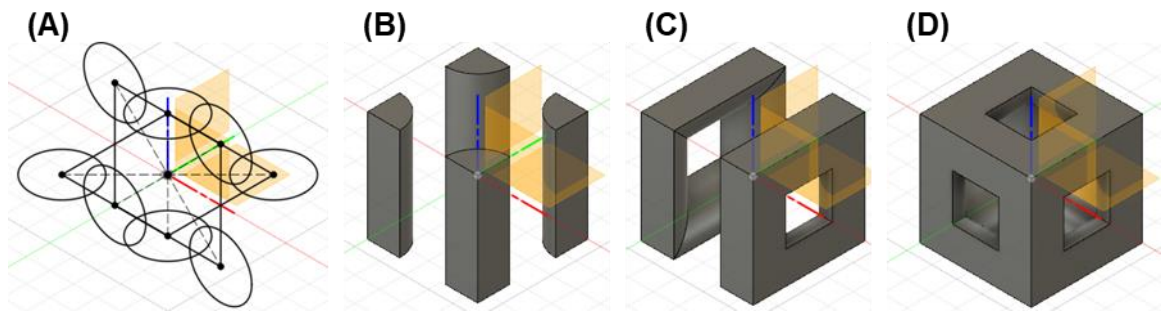


Figure 3: (A) 2-Dimensional cross-sectional sketches used to create a cubic unit cell in Fusion 360. (B) X-Y sketch extrusion into 3-dimensions. (C) X-Z sketch extrusion into 3-dimensions. (D) Y-Z sketch extrusion into 3-dimensions.

### 2.1.2 Workflow to Create a Kelvin Unit Cell

The complexity of Kelvin unit cell necessitates a different creation workflow than that of cubic unit cells. While it is feasible to analogously create 2-dimensional projections of a Kelvin geometry, the scope of this project limited the use of only the 2 Kelvin unit cell geometries which have been used experimentally in the Fromen Research Group. Since these geometries had been previously printed, mesh files of the void space of these unit cells were already available for use in Fusion 360. These meshes were imported into Fusion360, and a Boolean operation was used to produce the unit cell.

### 2.1.3 Surface Area Calculation

Fitting some theoretical pressure drop models requires a calculation of the internal surface area of the unit cell which is exposed to the internal flow. Determining this surface area requires a calculation using input from the Fusion360 model. This calculation is summarized below in Equation 7 for a cubic unit cell. The calculation is analogous for a Kelvin unit cell.

Equation 7: Internal surface area calculation for a cubic unit cell.  $A_{solid}$  = internal solid surface.  $A_{component}$  = the component surface area as determined by Fusion 360 CAD model.  $A_{cell}$  = the surface area of the bulk unit cell.  $A_{window}$  = the surface area of the window.

$$A_{solid} = A_{component} - 6(A_{cell} - A_{window})$$

## 2.2 Computational Fluids Dynamics

Computational fluid dynamics (CFD) is a numerical analysis method that is employed to simulate fluid flow in various systems.<sup>8,9</sup> CFD solvers numerically solve the partial differential equations (PDEs) that describe fluid flow, the Navier-Stokes equations. The Navier-Stokes equations describe the first principles conservation of momentum of fluid flow through infinitesimally discretized control volumes. For a Cartesian system, which is employed in this

project to describe the geometry of a unit cell, Equations 8 below show the Navier Stokes Equations, while Equation 9 shows the continuity equation, which described the conservation of mass of fluid. Since airflow velocities are simulated below 100 m/s, an incompressible CFD simulation is utilized. Additionally, while the unsteady dynamics of flow through unit cells and lattices may yield interesting phenomena, a steady state analysis is utilized for the simulations in this project.

Equation 8: Incompressible Navier-Stokes Equations of Conservation of Momentum.  $P$  = pressure.  $\tilde{\tau}$  = shear stress.  $g$  = acceleration due to gravity.

$$(A): \rho \left( \frac{\partial v_x}{\partial t} + v_x \frac{\partial v_x}{\partial x} + v_y \frac{\partial v_x}{\partial y} + v_z \frac{\partial v_x}{\partial z} \right) = -\frac{\partial P}{\partial x} + \left( \frac{\partial \tilde{\tau}_{xx}}{\partial x} + \frac{\partial \tilde{\tau}_{yx}}{\partial y} + \frac{\partial \tilde{\tau}_{zx}}{\partial z} \right) + \rho g_x$$

$$(B): \rho \left( \frac{\partial v_y}{\partial t} + v_x \frac{\partial v_y}{\partial x} + v_y \frac{\partial v_y}{\partial y} + v_z \frac{\partial v_y}{\partial z} \right) = -\frac{\partial P}{\partial y} + \left( \frac{\partial \tilde{\tau}_{xy}}{\partial x} + \frac{\partial \tilde{\tau}_{yy}}{\partial y} + \frac{\partial \tilde{\tau}_{zy}}{\partial z} \right) + \rho g_y$$

$$(C): \rho \left( \frac{\partial v_z}{\partial t} + v_x \frac{\partial v_z}{\partial x} + v_y \frac{\partial v_z}{\partial y} + v_z \frac{\partial v_z}{\partial z} \right) = -\frac{\partial P}{\partial z} + \left( \frac{\partial \tilde{\tau}_{xz}}{\partial x} + \frac{\partial \tilde{\tau}_{yz}}{\partial y} + \frac{\partial \tilde{\tau}_{zz}}{\partial z} \right) + \rho g_z$$

Equation 9: Continuity Equation

$$\frac{\partial \rho}{\partial t} + \left( v_x \frac{\partial \rho}{\partial x} + v_y \frac{\partial \rho}{\partial y} + v_z \frac{\partial \rho}{\partial z} \right) + \rho \left( \frac{\partial v_x}{\partial x} + \frac{\partial v_y}{\partial y} + \frac{\partial v_z}{\partial z} \right) = 0$$

For this project, an open-sourced CFD solver, OpenFoam was utilized to run CFD simulations. This solver was interfaced using an open-sourced graphical user interface (GUI), SimScale. SimScale uses a finite volume method, with nodes discretized over meshing elements, to solve the aforementioned PDEs that describe fluid flow.

### 2.2.1 Unit Cell Geometry and Meshing in SimScale

There are broadly two possible approaches to simulate fluid flow through or around an obstruction using a CFD solver. The “enclosure” approach consists of wrapping the obstruction in a larger “bounding box,” where the fluid domain encloses the obstruction and this larger

enclosure. This was initially the approach employed to simulate fluid flow through unit cells and lattices. However, numerical convergence issues and the increased computational costs associated with an increased fluid domain necessitated a change of approach. Instead, a “void space” approach was utilized, where the void space on the interior of a unit cell or lattice was taken as the fluid domain over which the CFD simulation is run. This approach leads to decreased computational costs and better numerical convergence. Figure 4 below highlights these different approaches schematically.

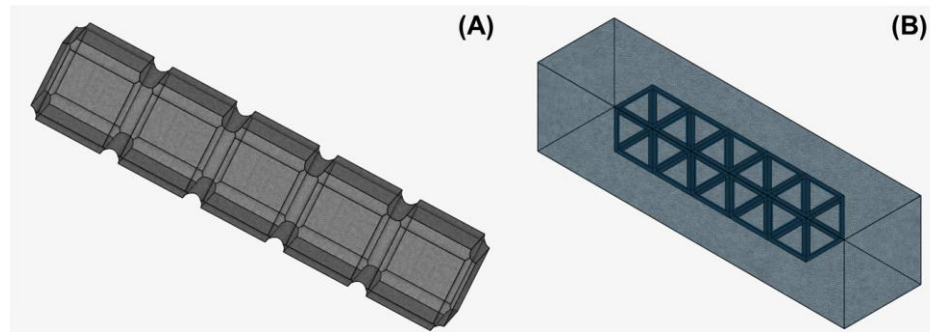


Figure 4: Schematic showing meshing approaches for CFD simulations of a sample cubic lattice. (A) Shows the “void space” approach which meshes only the fluid domain. (B) Shows the “enclosure” approach which meshes the solid lattice inside of an enclosure.

Meshing the fluid domain into discretized nodes is also a vital step in the workflow of CFD simulations. SimScale offers in-platform meshing capabilities that were leveraged in this project. The standard meshing algorithm accounts for both the physics of the simulation conditions and the geometry of the fluid domain to size the mesh. The surface mesh elements consist of exclusively triangular elements, while the interior of the mesh consists of exclusively hexahedral mesh elements. The transition between these layers is accounted for by tetrahedral

and pyramidal mesh elements.<sup>15</sup> To evaluate mesh quality after generating a mesh, SimScale provides guidelines in the software’s documentation<sup>15</sup>. The quality metrics are summarized below in Table 1.

Table 1: Mesh quality metrics for CFD

<b>Mesh Quality Metric</b>	<b>Threshold</b>
<i>Aspect ratio</i>	<<100
<i>Non-orthogonality</i>	<<75
<i>Edge ratio</i>	<<100
<i>Volume ratio</i>	<<100

For all meshes created, the quality metrics were verified to be below the quality thresholds suggested in the documentation.

### 2.2.2 CFD Simulation Boundary Conditions

Determining the appropriate boundary conditions of the CFD simulations required some iterative testing. Given the goal of the simulation is to test pressure drop for a given flow condition, a velocity inlet-pressure outlet boundary condition was determined to be the most appropriate inlet-outlet combination. The faces of a unit cell or lattice void space that border the struts of a unit cell or lattice (lattice-normal faces) were assigned a “no-slip” boundary condition, given that flow would not penetrate these solid faces. Based on literature, it was determined that setting the “open” faces of the void space, or the faces that are open to the flow boundary but are not the inlet or outlet, should be assigned a “free slip” boundary condition<sup>7,8</sup>. This is because these faces do experience flow, but the flow phenomena normal to these faces is not of interest to the simulations investigating flow parallel to these faces. Thus, a free-slip



boundary condition, which allows for flow parallel to the plane of the face but sets flow in the directs normal to the plane to zero, was deemed as the most appropriate boundary condition. The boundary conditions are summarized below in Figure 5.

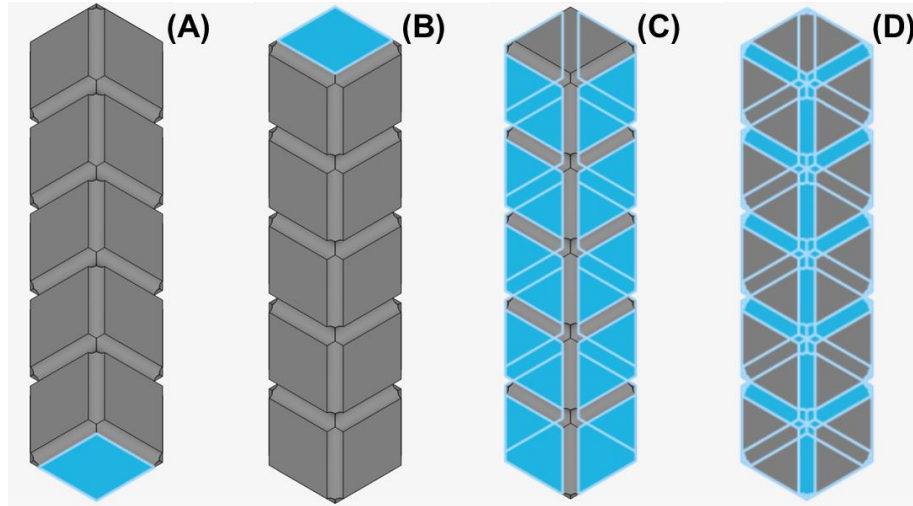


Figure 5: Simulation boundary conditions for CFD simulations. (A) Velocity inlet, (B) pressure outlet, (C) slip (no penetration) on open faces, (D) no slip on lattice-normal faces.

### 2.2.3 Turbulence Modeling, Numerical Conditions, and Convergence

The k-omega shear stress transport (SST) turbulence model was utilized as the turbulent algorithm for CFD simulations. K-omega SST is commonly used for low-Re flow conditions because the model is stable down to the viscous sub-layer. Given the low-Re conditions utilized in this project, this model is an appropriate selection.

Several numerical conditions were also selected for CFD simulations. The residual tolerance controls for calculated properties, including velocity, pressure, turbulent kinetic energy, and specific dissipation rate were all selected to be  $10^{-7}$ , based on SimScale

documentation. The smooth solver was selected to solve all properties with the exception of pressure, which relied on the GAMG solver, based on the standard recommendation from SimScale and OpenFoam documentation.<sup>15</sup> Simulations were deemed to reach numerical convergence when residuals for flow properties fell below  $10^{-3}$  to a steady value. This is based off of accepted literature convergence thresholds. Figure 6 below shows a sample converged residual plot for a CFD simulation of flow through a lattice structure.

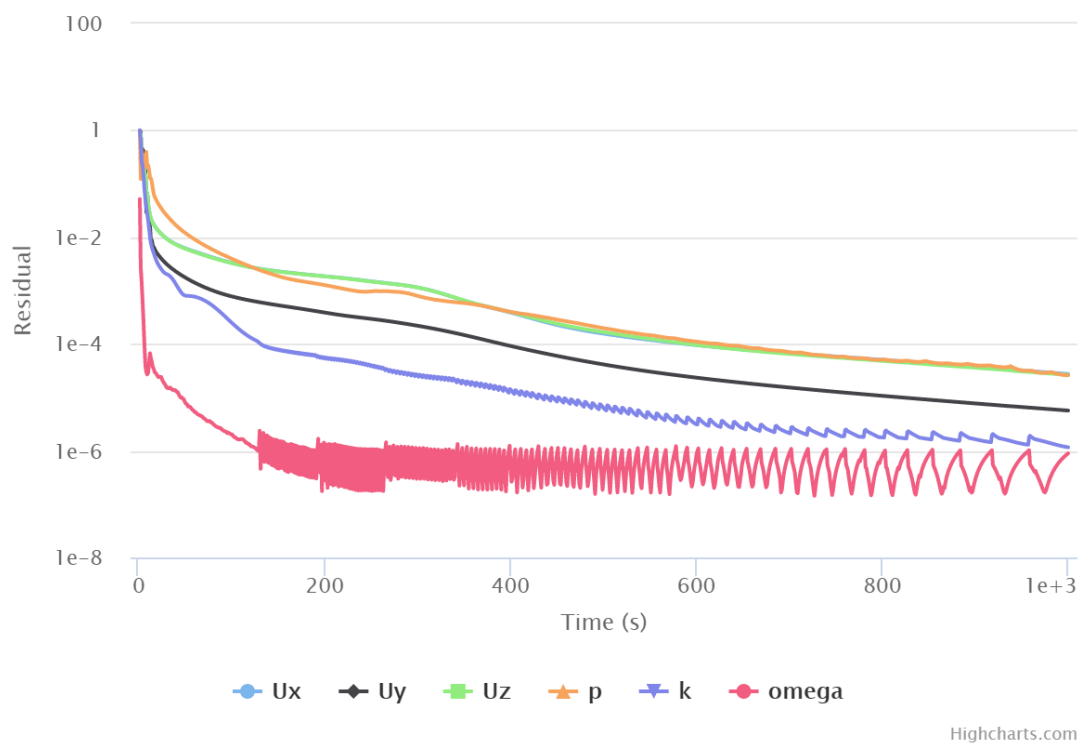


Figure 6: Sample residual convergence plot. Residuals for all properties reach a steady value below  $10^{-4}$ . Slight oscillations in the range of  $10^{-7}$  are tolerable.

### 2.2.3.1 Mesh Independence

Mesh independence was asserted for all CFD simulations. The purpose of mesh independence is to verify that the discretization of the geometry into a mesh is not arbitrarily influencing the simulations results<sup>16</sup>. To verify mesh independence, the number of cells in a mesh (mesh size) is increased until the quantitative result of interest, outlet pressure, changes less than 1% for a further increase in the mesh size<sup>16</sup>. SimScale offers a qualitative metric for mesh size, called mesh fineness, which was used a proxy for mesh size once mesh independence was established using the number of cells.

For a cubic system, the mesh independence for constant strut radius is shown below in Figure 7.

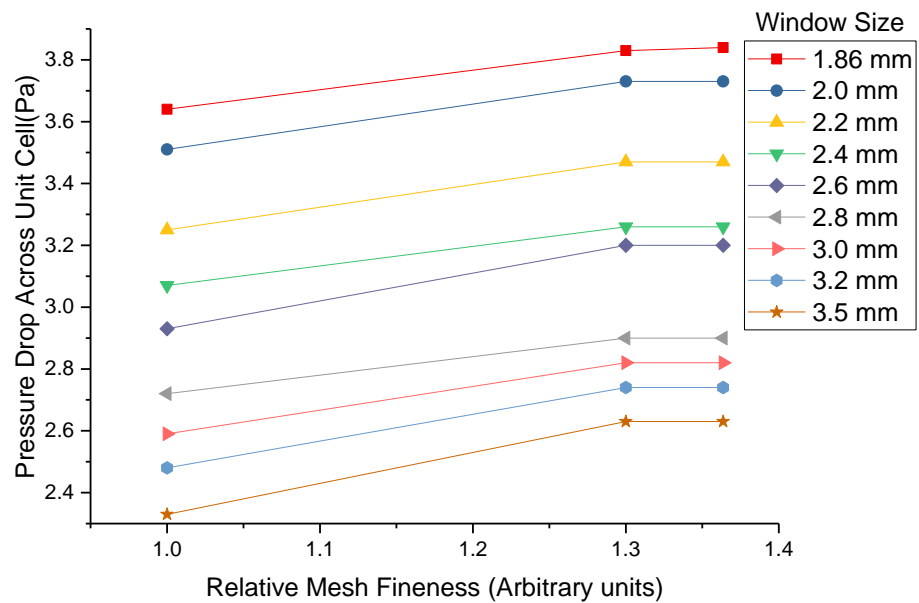


Figure 7: Mesh independence study for cubic unit cells in the constant strut radius dataset. The pressure drop was determined to change under 0.1% for all unit cells.

Figure 7 shows that upon a relative mesh fineness of 1.36, the pressure drop change was less than 0.1% for all unit cells, allowing us to claim the results were quantitatively mesh independent for meshes at this relative fineness. Meshes for cubic unit cells were ensured to be at least generated at this level of fineness. This same process was repeated for the two Kelvin unit cells studied, and the results are shown below in Figure 8.

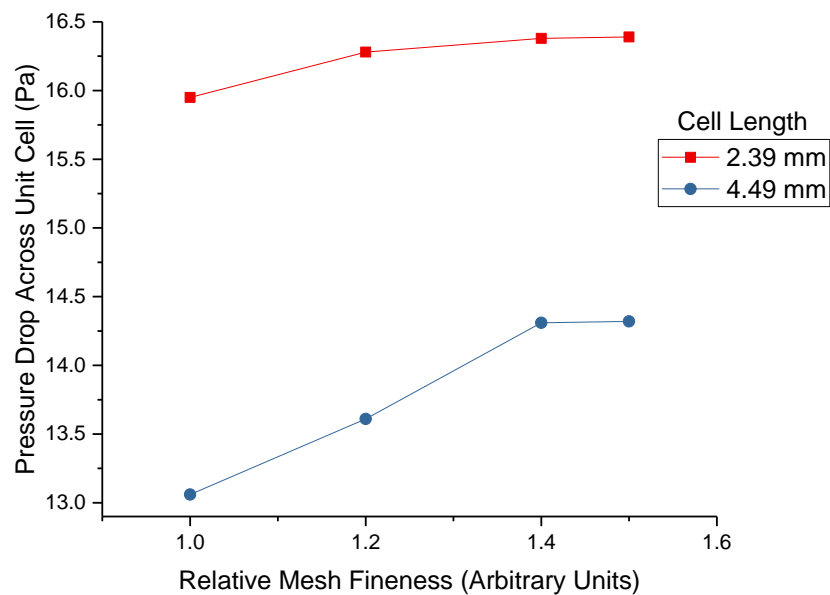


Figure 8: Mesh independence study for Kelvin unit cells. The pressure drop was determined to change under 0.1% for all unit cells.

Figure 8 shows that upon a relative mesh fineness of 1.5, the pressure drop change was less than 0.1% for all unit cells, allowing us to claim the results were quantitatively mesh independent for meshes at this relative fineness. Meshes for Kelvin unit cells were ensured to be at least generated at this level of fineness.

#### 2.2.4 Plot Generation and Statistical Analysis in OriginLab

The scientific software Origin(Academic) Version 2017, licensed by OriginLab, was utilized to generate the plots shown in this project<sup>17</sup>. Statistics including regression, root mean square error (RMSE), and ANOVA were completed in OriginLab. RMSE is shown below in Equation 10.

Equation 10: Root Mean Square Error (RMSE).  $N = \text{number of observations}$ .  $y_i = \text{observed values}$ .  $\hat{y}_i = \text{predicted values}$ .

$$RMSE = \sqrt{\frac{\sum_{i=1}^N (y_i - \hat{y}_i)^2}{N}}$$

For linear and logistic regression,  $r_{adjusted}^2$  values are reported. ANOVA is used to compare the statistical significance of the slope of generated linear regressions, and p-values are reported for these tests.

## Chapter 3

### RESULTS AND DISCUSSION

#### 3.1 Flow Visualization through Single Unit Cell

First, the flow through a single unit cell was qualitatively characterized to investigate the flow phenomena observed. This was done for both a cubic and Kelvin unit cell of analogous geometries that have both been experimentally tested in the Fromen Research Group. The flow condition was selected via matching a superficial velocity in the cubic unit cell that had been tested experimentally. Then, the flow rate was conserved between the cubic and Kelvin unit cells, leading to a different superficial velocity and Reynolds number between the two cells. The geometries and flow conditions of each for each unit cell type are summarized below in Table 2.

Table 2: Unit cell geometries and flow conditions used for flow visualization through single unit cells.

Property	Cubic Unit Cell	Kelvin Unit Cell
Cell Length (mm)	2.39	2.39
Strut Radius (mm)	0.26	0.262
Window Size (mm <sup>2</sup> )	3.46	3.81
Flow Rate (L/s)	578	578
Superficial Fluid Velocity (m/s)	2.00	2.20
Re <sub>window</sub>	243	207

### 3.1.1 Cubic Unit Cell

The cubic unit cell geometry described in Table XX was simulated under the flow condition with a superficial inlet air velocity of 2 m/s. The velocity contours for the overall velocity and the two directions transverse to flow (X and Y) were taken at the inlet, outlet, and a dimensionless distance in the flow direction of 0.25, 0.5, and 0.75. The velocity contours for the flow direction vector component (Z direction) were not included, as they are identical in relative magnitude to the overall velocity contours. These velocity contours are shown below in Figure 10.

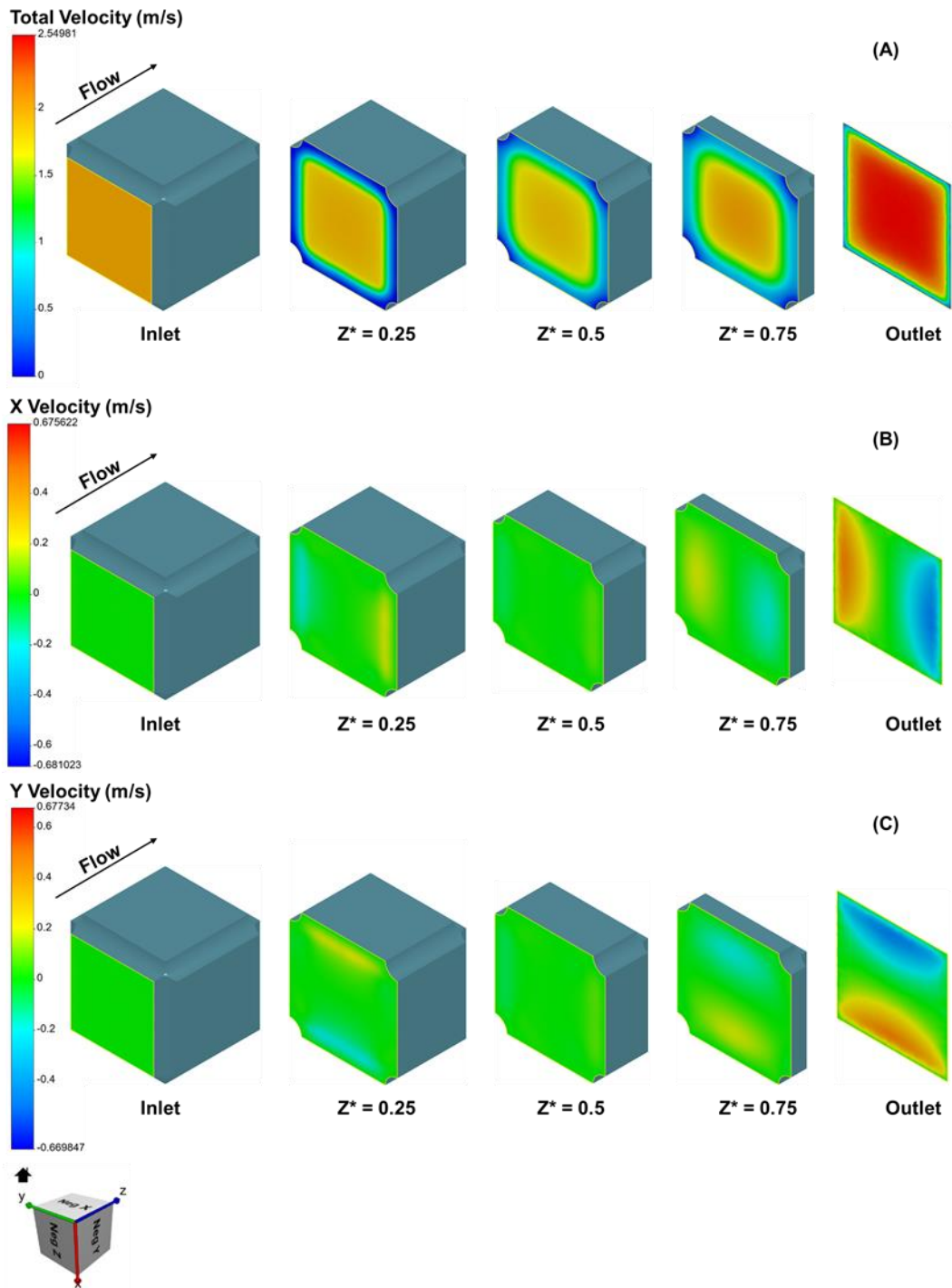


Figure 10: Flow visualization through a cubic unit cell.



Overall, the flow visualization suggests that velocity contours through the unit cell follow expected dynamics. The overall and flow direction velocity experience a “flow conditioning” or “pore focusing” effect through the center of the unit cell as the hydraulic diameter shrinks due to the presence of struts. Ultimately, the maximum velocity is experienced at the outlet, with a maximum magnitude of 2.55 m/s.

In the transverse directions, the flow also follows the dynamics expected for flow around cylindrical obstructions<sup>18,19</sup>. We expect that transverse flow will form to satisfy the no-slip condition on the struts. For the struts in the X-Z plane, symmetrical transverse flow in the X-direction develops as the flow approaches the struts. Similarly, for struts in the Y-Z plane, symmetrical transverse flow in the Y-direction develops as the flow approaches the struts. The magnitude of this transverse flow is the largest at the outlet, after the flow encounters the second set of X-Z and Y-Z struts. The largest magnitude of Y-directional flow velocity is 0.68 m/s, while the largest magnitude of X-directional flow velocity is 0.67 m/s. This small differences in magnitude between the Y- and X- directional flow velocity are likely due to the distribution of nodes across the mesh.

### **3.1.2 Kelvin Unit Cell**

The Kelvin unit cell geometry described in Table 2 was simulated under the flow condition with a superficial inlet air velocity of 2.2 m/s. The velocity contours for the overall velocity and the two directions transverse to flow (X and Y) were taken at the inlet, outlet, and a dimensionless distance in the flow direction of 0.25, 0.5, and 0.75. The velocity contours for the flow direction vector component (Z direction) were not included, as they are identical in relative magnitude to the overall velocity contours. These velocity contours are shown below in Figure 11.

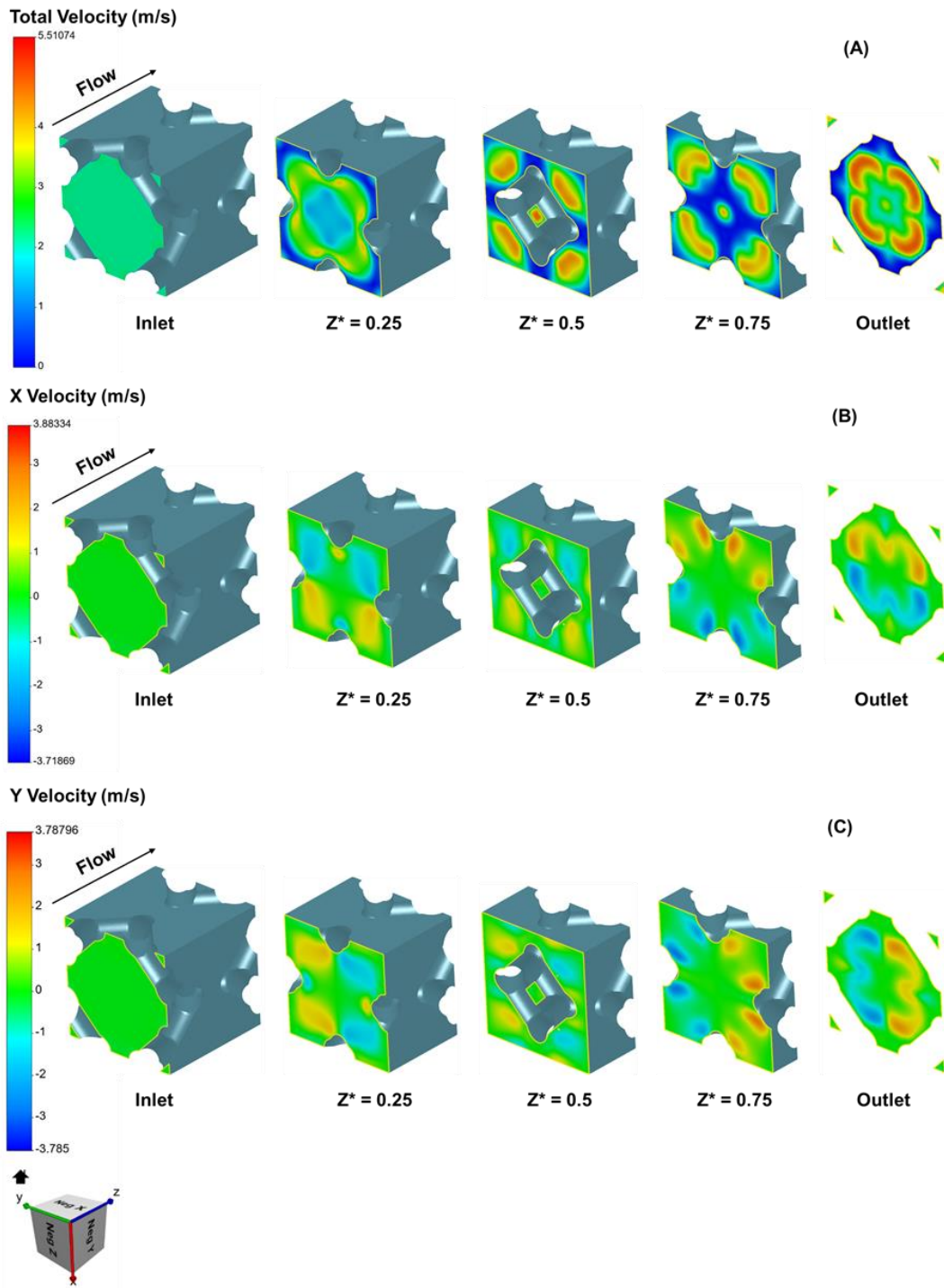


Figure 11: Flow visualization through a Kelvin unit cell

Overall, the flow visualization in Figure 11 again suggests that the simulation follows expected dynamics. Like the cubic unit cell, the overall and flow direction velocity experience a “flow focusing” or “pore focusing” effect through the center of the unit cell as the hydraulic diameter shrinks due to the presence of struts. However, unlike for the cubic unit cell, this effect is also reproduced through the peripheral pores as well as for the inner pore. Figure 12 below shows the 2-dimensional inlet face of the Kelvin cell to demonstrate the inner pore and windows that provide channels for flow focusing. Ultimately, the maximum velocity is experienced at the outlet, with a maximum magnitude of 5.51 m/s. Compared to the cubic cell, the magnitude of the increase in velocity is dramatically larger.

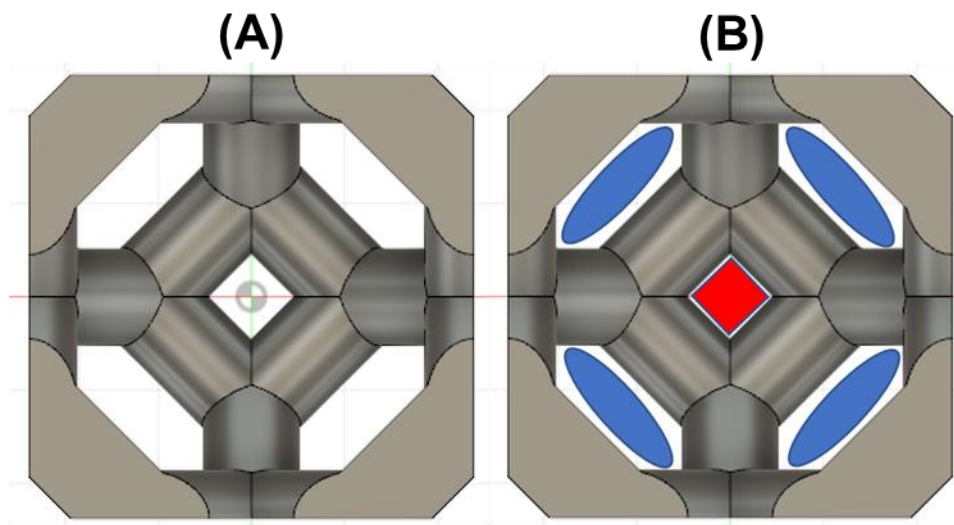


Figure 12: Inlet face of the Kelvin unit cell. (A) Shows 2-dimensional projection of the inlet. (B) Highlights the pores through which flow focusing is observed. Blue ovals rest in the peripheral pores, while the red square fills the central pore.

In the transverse directions, the flow also follows the dynamics expected for flow around cylindrical obstructions<sup>18,19</sup>. We expect that transverse flow will form to satisfy the no-slip condition on the struts. For the struts in the X-Z plane, symmetrical transverse flow in the X-direction develops as the flow approaches the struts. Similarly, for struts in the Y-Z plane, symmetrical transverse flow in the Y-direction develops as the flow approaches the struts. The magnitude of this transverse flow is the largest at the outlet, after the flow encounters the second set of X-Z and Y-Z struts. The largest magnitude of Y-directional flow velocity is 0.68 m/s, while the largest magnitude of X-directional flow velocity is 0.67 m/s. This small differences in magnitude between the Y- and X- directional flow velocity are similarly likely due to the distribution of nodes across the mesh.

### **3.2 Cubic-based Lattice Pressure Drop vs. Window Size**

The goal of this set of experiments was to probe the effects of cubic unit cell geometry on pressure drop. Specifically, a window size range was developed between the window size values for the experimentally-tested cubic unit cells. The window sizes were chosen to be evenly spaced, incremented by 0.20 mm between 2.00 and the upper limit of 3.50 mm (based on the larger experimentally-tested unit cell). For this range of window sizes, two sets of lattice designs were generated:

- (1) For a constant strut radius equal to the smaller experimental cubic strut radius, the cell length was varied to achieve the desired window sizes.
- (2) For a constant cell length radius equal to the larger experimental cubic cell length, the strut radius was varied to achieve the desired window sizes.

Table 3 below summarizes the resulting geometries for these datasets.

Table 3: Designs for Constant Cell Length and Strut Radius Designs

<i>Window Size (mm)</i>	<b>Constant Strut Radius</b>		<b>Constant Cell Length</b>	
	<i>Cell Length (mm)</i>	<i>Strut Radius (mm)</i>	<i>Cell Length (mm)</i>	<i>Strut Radius (mm)</i>
1.86	2.385	0.262	4.487	1.314
2.00	2.525	0.262	4.487	1.244
2.20	2.725	0.262	4.487	1.144
2.40	2.925	0.262	4.487	1.044
2.60	3.125	0.262	4.487	0.944
2.80	3.325	0.262	4.487	0.844
3.00	3.525	0.262	4.487	0.744
3.20	3.725	0.262	4.487	0.644
3.50	4.025	0.262	4.487	0.494

The unit cell designs in the constant strut radius (CSR) and constant cell length (CCL) datasets are referenced by their window size (*e.g.*, CSR\_1.86 or CCL\_1.86). For the geometries in each of these datasets, the volume porosity ( $\epsilon_o$ ) was calculated according to the relationship shown below in Equation 11.

Equation 11: Open-cell volume porosity

$$\epsilon_o = 1 - \frac{V_{solid}}{V_{bulk}}$$

The volume porosities were then plotted against the window sizes for each set of unit cells. The results are shown below in Figure 13.

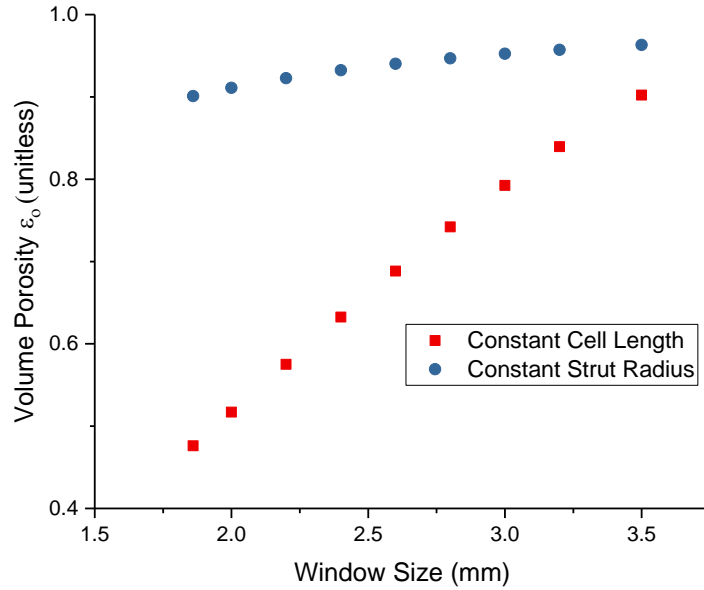


Figure 13: Volume Porosity for both the constant cell length and constant strut radius. For CCL, linear regression yields an  $r^2_{\text{adjusted}} = 0.996$ . For CSR, linear regression yields an  $r^2_{\text{adjusted}} = 0.952$ , and a logarithmic fit yields  $r^2_{\text{adjusted}} = 0.986$ .

Figure 13 demonstrates the range of volume porosity values observed in each dataset. For the CCL dataset, volume porosities ranged from 0.476 to 0.902. For the CSR dataset, volume porosities ranged from 0.901 to 0.963. The different ranges of volume porosities between these datasets are a useful distinction towards understanding when various theoretical pressure drop correlations may be appropriate to use, and where pressure drop correlations may fail to accurately predict pressure drop. The rates of increase with window size also differs between the two datasets. For the CCL dataset, we expect and observe a linear relationship, since  $V_{bulk}$  remains constant, while the  $V_{solid}$  will decrease linearly as window size increases (decreasing strut size), leading to a linear increase in  $\epsilon_0$  ( $r^2_{\text{adjusted}} = 0.996$ ). For the CSR dataset, we expect and observe a non-linear logarithmic relationship.  $V_{bulk}$  increases according to the

cube of increasing window size (increasing cell length), but  $V_{solid}$  increases according to a fraction scaled to the cube of the window size. Thus, the ratio of  $V_{solid}$  to  $V_{bulk}$  will decrease non-linearly, leading to a non-linear increase in  $\varepsilon_o$  with window size. This is supported by the statistical regressions run on this dataset, where a linear fit yielded an  $r^2_{adjusted} = 0.952$ , but a logarithmic fit yielded an  $r^2_{adjusted} = 0.986$ .

Next, the total volume-based specific surface area ( $SSA_{volume}$ ) was calculated for both the CSR and CCL datasets according to Equation 12, shown below.  $SSA_{volume}$  is a geometric parameter that is needed to fit several theoretical pressure drop models.

Equation 12: Total volume-based specific surface area for a cubic unit cell

$$SSA_{volume} = \frac{A_{solid}}{V_{bulk}}$$

The  $SSA_{volume}$  for both datasets is plotted against window size below in Figure 14.

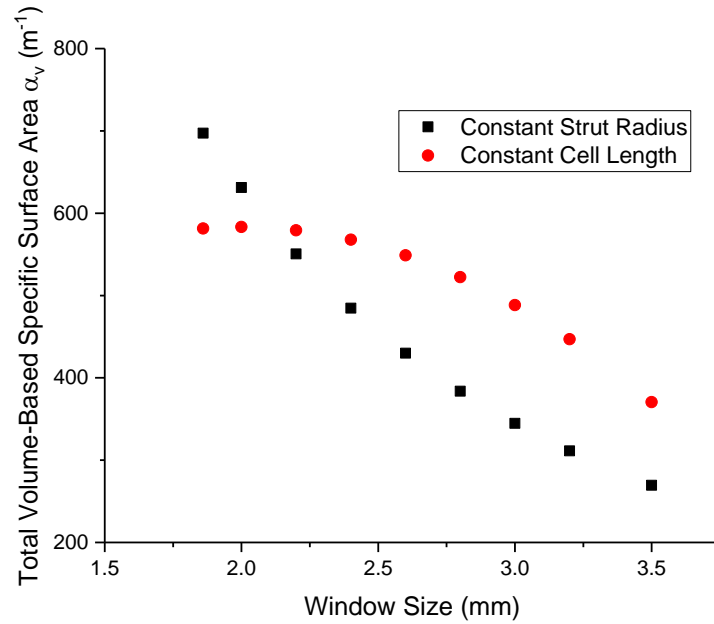


Figure 14: Volume-based surface area for CSR and CCL unit cell designs

From Figure 14, the relationship between  $SSA_{volume}$  for each dataset is observed. For CCL,  $V_{bulk}$  is constant, but  $A_{solid}$  scales with the square of window size, leading to an exponentially decreasing  $SSA_{volume}$ . In contrast, for CSR,  $V_{bulk}$  increased according to the cube of window size, while  $A_{solid}$  increases according to a fraction of the cube of window size, leading to a decaying decrease in  $SSA_{volume}$ .

The trends that the CSR and CCL datasets exhibit for  $SSA_{volume}$  are important towards understanding where different theoretical models might be most appropriate to fit, or where they might deviate from the CFD simulations predictions. The icPOCS model, for example, was validated against experimental data for a range of  $SSA_{volume}$  values between 540 – 2100 m<sup>-1</sup>, while the range of both the CSR and CCL datasets reaches values of 269 m<sup>-1</sup>. Given that greater pressure drop will be induced for larger values of  $SSA_{volume}$ , it is reasonable to expect that



there might be challenges associated with fitting theoretical models to the lower range of  $SSA_{volume}$  values in both the CSR and CCL datasets.

### **3.2.1 CFD Results**

After characterizing the unit cell geometries of these datasets, CFD simulations were run on each unit cell to determine how pressure drop varies with window size. To probe the effects of flow conditions on the pressure drop results, two conditions were tested across both datasets: (1) a constant  $Re_{window} = 750$  and (2) a constant superficial velocity of 3.28 m/s. As previously described, appropriate theoretical pressure drop correlations were fit to the geometries and flow conditions and compared to the CFD results.

#### **3.2.1.1 Constant Strut Radius Experiment**

Figure 15 below shows the CSR CFD results for the flow condition of constant  $Re_{window} = 750$ . Table 4 below summarizes the root mean square error (RMSE) for each model fit compared to the CFD results.

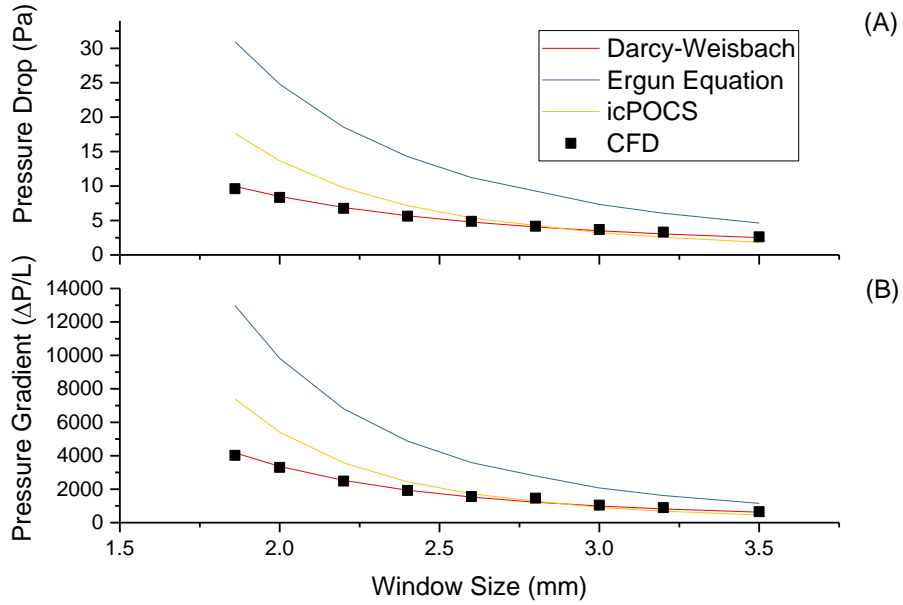


Figure 15: Results from CFD simulations for the CSR dataset for a constant flow condition of  $Re_{window} = 750$ . (A) Pressure drop across unit cell. (B) Pressure gradient across unit cell.

Table 4: RMSE values for model fits of CSR simulations under  $Re_{window} = 750$

Model	RMSE	
	Pressure Drop $\Delta P$ (Pa)	Pressure Gradient $\Delta P/L$ (Pa/m)
<i>Darcy-Weisbach</i>	0.139	102
<i>Ergun Equation</i>	10.7	4,190
<i>icPOCS</i>	3.43	1,390

Figure 15 shows that for the constant flow condition of a  $Re_{window} = 750$ , the Darcy-Weisbach model offered best model fit compared to Ergun and icPOCS models. The calculated RMSE values also show that both the Ergun and icPOCS models drastically overestimate the pressure drop over lattice length at lower window  $\Delta$  size values. Particularly, below window sizes

of 2.5 mm, these models both overestimate the pressure drop by a substantial amount. At larger window sizes, the icPOCS model predictions converge towards the CFD results. It is important to note that the range of volume porosities for this dataset (all  $> 0.90$ ) should be high enough for the icPOCS model to be a reasonable predictor. However, we do observe a poor model fit, suggesting either that icPOCS could potentially be sensitive to both total lattice length or flow condition, neither of which have been probed experimentally in the model's development. The poor model fit for Ergun is likely due to the length scale of the total lattice length being below the traditional lengths to which Ergun has been applied.

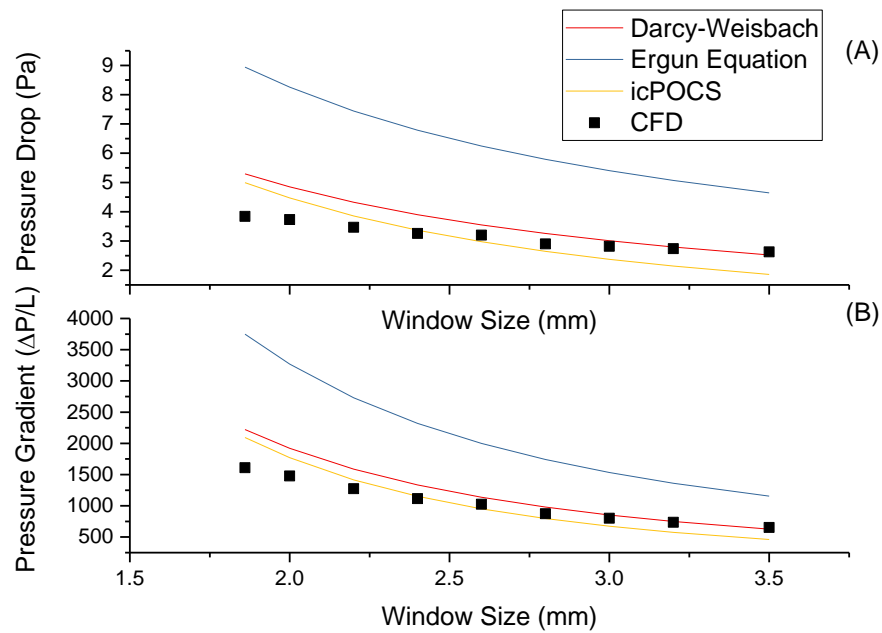


Figure 16: Results from CFD simulations for the CSR dataset for a constant flow condition of  $V_{superficial} = 3.28 \text{ m/s}$ . (A) Pressure drop across unit cell. (B) Pressure gradient across unit cell.

Table 5: RMSE values for model fits of CSR simulations under  $V_{superficial} = 3.28 \text{ m/s}$ .

Model	RMSE	
	Pressure Drop $\Delta P$ (Pa)	Pressure Gradient $\Delta P/L$ (Pa/m)
<i>Darcy-Weisbach</i>	0.732	288
<i>Ergun Equation</i>	3.47	1,260
<i>icPOCS</i>	0.606	219

Figure 16 shows that for constant  $V_{superficial} = 3.28 \text{ m/s}$  through the unit cell inlets, the icPOCS model offered the best predictions. The RMSE values show that the pressure drop prediction differed from the CFD value by about 0.61 Pa, while the length-normalized gradient differs by about 219 Pa/m, as shown in Table 5. The Darcy-Weisbach offers a similar fit in terms of magnitude of the error from the CFD results, but is overall slightly worse than the icPOCS model. The Ergun model again drastically overestimates the pressure drop, likely again because of the total length scale of an individual unit cell is relatively small.

The icPOCS model fit for the constant superficial velocity is dramatically improved over the constant  $Re_{window}$ , suggesting that the icPOCS model may fit best under specific fluid velocities, specifically smaller velocities. For constant  $Re_{window}$ , the fluid velocities increase to 6.17 m/s as window size decreases, suggesting that the icPOCS model fidelity degrades at higher fluid velocities.

### 3.2.1.2 Constant Cell Length Experiment

For the CCL dataset, pressure drop was determined over the cell length, and again the Darcy-Weisbach model, Ergun Equation, and icPOCS model were fitted to the flow conditions and unit cell geometries. Figure 17 below shows the pressure drop vs window size results for the constant  $Re_{window} = 750$ . Figure 18 shows the pressure drop vs window size for the

$V_{superficial} = 3.28 \text{ m/s}$  flow condition. The pressure gradient is not included, since for the constant cell length, the gradient and pressure drop are scaled by the same factor and thus provides no new information. Table 6 below summarizes the RMSE for each flow condition.

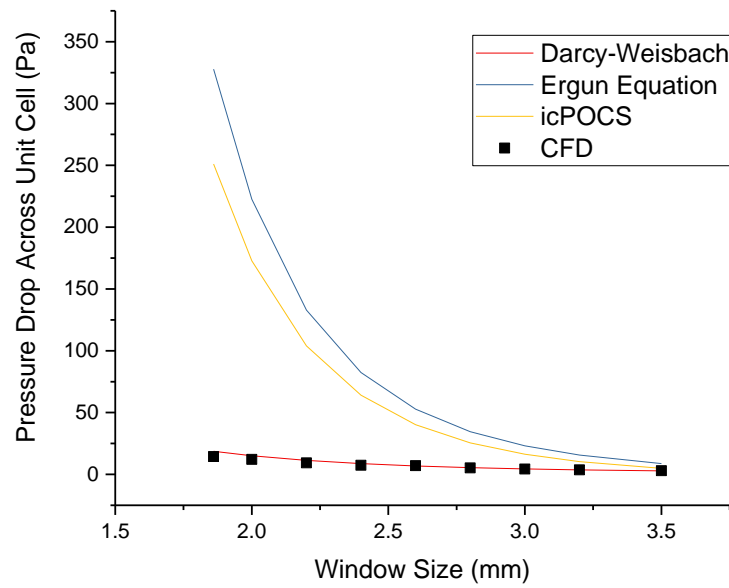


Figure 17: Results from CFD simulations for the CSR dataset for a constant flow condition of  $Re_{window} = 750$ .

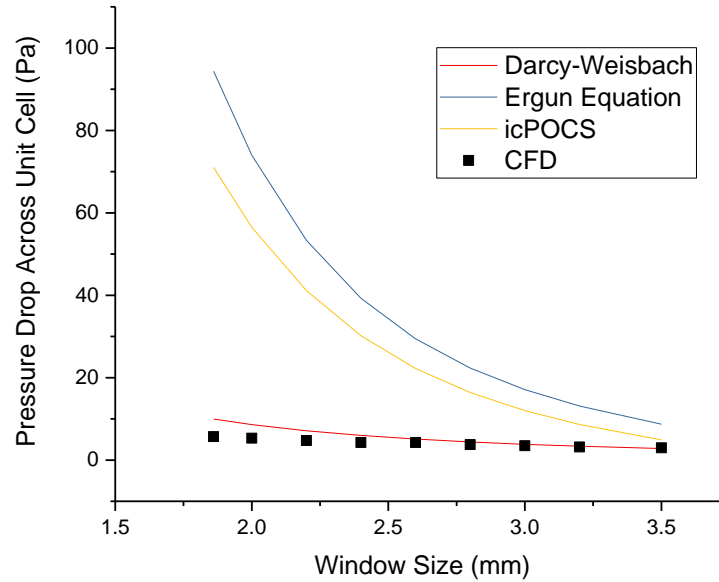


Figure 18: Results from CFD simulations for the CSR dataset for a constant flow condition of  $V_{superficial} = 3.28 \text{ m/s}$ .

Table 6: RMSE values for model fits of CCL simulations.

Model	RMSE for Pressure Drop $\Delta P$ (Pa)	
	$Re_{window} = 750$	$V_{superficial} = 3.28 \text{ m/s}$
<i>Darcy-Weisbach</i>	1.94	2.08
<i>Ergun Equation</i>	136	44.0
<i>icPOCS</i>	103	32.4

Figures 17 and 18 show that for the CCL unit cell datasets, the Darcy-Weisbach model provides the best model fit, regardless of the flow condition. Table 6 shows that the Darcy-Weisbach model predictions differ from the CFD results by about 1.9 Pa for the  $Re_{window} = 750$  condition and 2.1 Pa for the  $V_{superficial} = 3.28 \text{ m/s}$  condition. Both the Ergun Equation and the icPOCS model several overestimate the CFD results, again particularly

at the lower porosity values (corresponding to smaller window sizes). There is virtually no qualitative difference in model fits observed between the different flow conditions, unlike for the CSR dataset. It is again surprising that the icPOCS model does not offer a robust prediction for pressure drop over cubic unit cells, since the model was developed and validated specifically for cubic unit cells. However, these results suggest that the length scale of individual unit cells or the smaller volume porosity values introduce an additional complexity to the fluid transport for which the icPOCS model is unable to account.

### **3.2.2 Volume porosity as a pressure drop predictor**

The role of volume porosity as a predictor of pressure drop has been explored and suggested in literature.<sup>3,4,6</sup> For each of the CCL and CSR datasets, the volume porosity was plotted against the pressure drop in each of the flow condition experiments. Linear regression was performed to determine the feasibility of using volume porosity as a linear predictor of pressure drop. This analysis is included below in Figure 19.

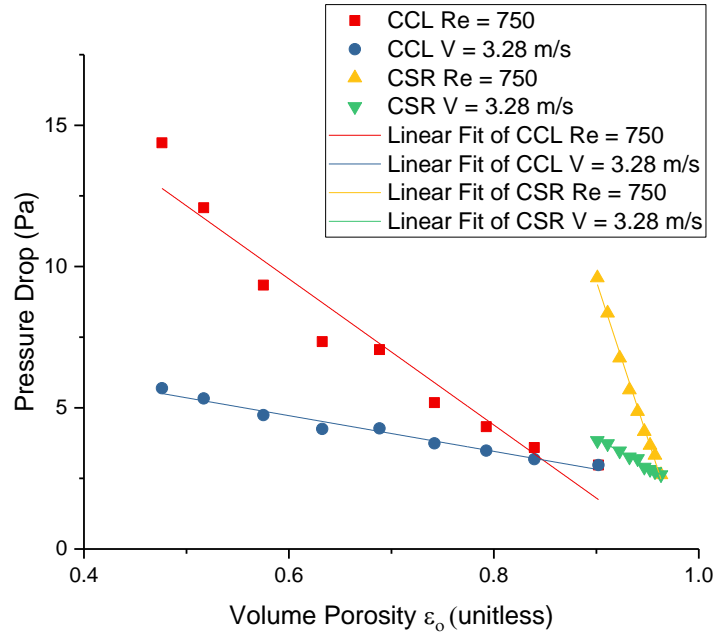


Figure 19: Pressure Drop vs Volume Porosity for the CSR and CCL experiments. For CCL  $Re = 750$ , linear regression yields an  $r^2_{\text{adjusted}} = 0.930$ . For CCL  $V = 3.28 \text{ m/s}$ , linear regression yields an  $r^2_{\text{adjusted}} = 0.972$ . For CSR  $Re = 750$ , linear regression yields an  $r^2_{\text{adjusted}} = 0.994$ . For CSR  $V = 3.28 \text{ m/s}$ , linear regression yields an  $r^2_{\text{adjusted}} = 0.985$ .

Figure 19 shows that the results suggest that under specific flow conditions, volume porosity is able function as a linear predictor of pressure drop. Specifically, the CSR dataset (which has volume porosities  $> 0.9$ ) shows a highly linear relationship between pressure drop and volume porosity, with  $r^2_{\text{adjusted}} = 0.994$  for  $Re_{\text{window}} = 750$  and  $r^2_{\text{adjusted}} = 0.985$  for  $V_{\text{superficial}} = 3.28 \text{ m/s}$ . This suggests that for highly porous lattices, potentially only volume porosity is needed to predict pressure drop to a high fidelity. While this does not negate the need for a robust theoretical correlation, it does offer promise as a predictive tool under specific conditions.



### 3.3 Lattice Negative Flow Decoupling

The goal of this experiment was to test how pressure drop profiles evolve with increasing unit cells in the flow direction. This is important, specifically, for the optimization of lattice designs. If it were determined that pressure drop is “coupled” to successive unit cells, the optimization algorithm would need a mechanistic way to determine flow coupling.

Thus, following the investigation of how geometry and flow conditions influence pressure drop through single unit cells, the effects of lattice configuration were explored. For the experimentally-tested Kelvin and cubic unit cells visualized in Chapter 3.1, lattices were configured with varying numbers of unit cells in the flow direction. Specifically, in the flow direction,  $N \in [1,5]$ , where N is the number of unit cells. The flow conditions tested were the same conditions as tested in Chapter 3.1, and the inlet boundary conditions and unit cell geometry can be found in Table 2.

#### 3.3.1 Cubic-based lattice

Figure 20 below shows the results for pressure drop over lattice length for the cubic lattice configurations. Since the lattices are made of repeating unit cells with identical geometry, the X-axis shows lattice length, but each design is incremented by cell length. The Darcy-Weisbach model, Ergun Equation, and icPOCS models are all fit to the flow condition and lattice geometry to compare to the CFD results. Table 8 shows the RMSE values for the model fits.

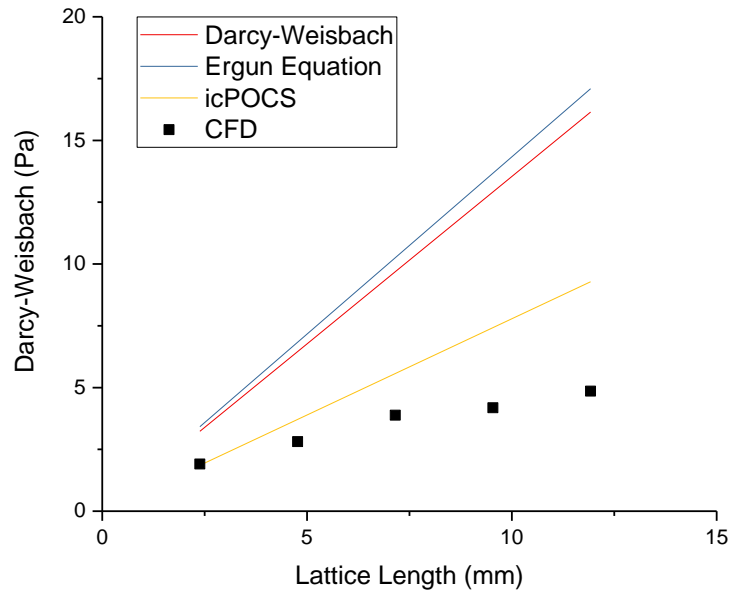


Figure 20: Pressure drop for cubic lattices comprised of 1-5 unit cells in the axial direction. Model fits for the Darcy-Weisbach, Ergun Equation, and icPOCS models are included.

Table 8: RMSE values for model fits of cubic lattice simulations.

	RMSE for Pressure Drop $\Delta P$ (Pa)
<b>Model</b>	$V_{superficial} = 2 \text{ m/s}$
<i>Darcy-Weisbach</i>	5.30
<i>Ergun Equation</i>	7.19
<i>icPOCS</i>	3.36

Figure 20 shows that the icPOCS model offers the best model fit over the length of the lattice. From Table 8, we see that the RMSE value shows that the icPOCS model predicts pressure drop within about 3.4 Pa on average. The Ergun Equation and Darcy-Weisbach model both overestimate the pressure drop for all of the lattice designs.

Next, the pressure drop after the Nth unit cell was determined in order to determine if changing the lattice configuration changes the pressure drop profiles. For example, if pressure drop after the 1<sup>st</sup> unit cell in the lattice increased as the number of unit cells in axial direction increased, we would have to mechanistically quantify how additional unit cells increase pressure drop. On the other hand, if pressure drop after the 1<sup>st</sup> unit cell is constant for a fixed flow condition, we can disregard the effects of positional orientation when developing an optimization algorithm for a lattice design. Figure 21 below shows the pressure drop after the Nth unit cell for all lattice designs.

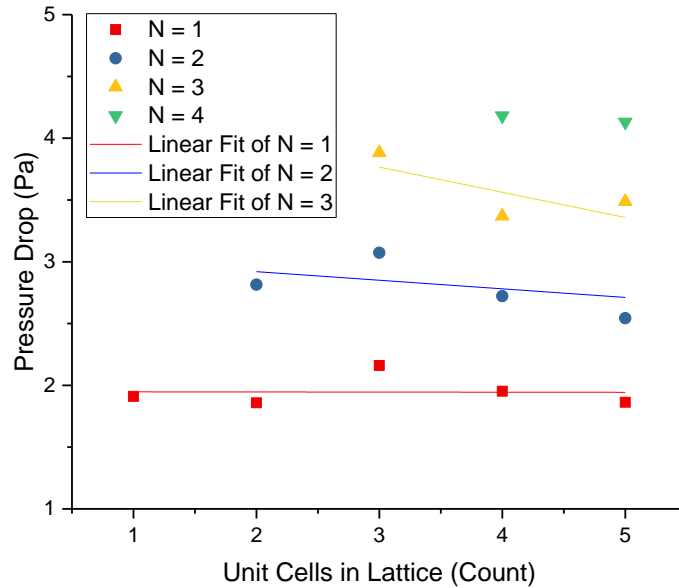


Figure 21: Pressure drop decoupling after Nth unit cell for cubic lattice stack. ANOVA tested statistical difference between regression slopes and 0. N = 1 p-value = 0.985. N = 2 p-value = 0.515. N = 3 p-value = 0.494.

Figure 21 shows that pressure is quantitatively decoupled over cubic lattice structures with up to 5 unit cells in the axial direction for the flow condition of inlet flow velocity of 2 m/s. Each series in Figure 21 represent pressure drop after the corresponding unit cell (N = 1, N = 1, ...). For pressure drop after the first, second, and third unit cells, a linear regression was performed in OriginLab. Regression could not be performed for pressure drop after the fourth and fifth unit cells, since lattices were only tested up to 5 unit cells in axial direction. The slope of the linear regressions were compared to 0 using an ANOVA test as described in Chapter 2.2.4. For all three of the regressions performed, the slopes were not statistically different from 0, with p-values for significance of  $p = 0.985$ ,  $0.515$ , and  $0.494$  for pressure drop after the first, second, and third unit cells, respectively.

These results importantly suggest that, at least for cubic unit cells of this geometry, pressure drop is at least decoupled under this flow condition up to the fourth unit cell. This is a vital conclusion that allows for the integration of these lattice structures into a data-driven optimization workflow.

### **3.3.2 Kelvin-based lattice**

Figure 22 below shows the results for pressure drop over lattice length for the Kelvin lattice configurations. Since the lattices are made of repeating unit cells with identical geometry, the X-axis shows lattice length, but each design is incremented by cell length. The Darcy-Weisbach model, Ergun Equation, and Foam models are all fit to the flow condition and lattice geometry to compare to the CFD results. Table 9 shows the RMSE values for the model fits.

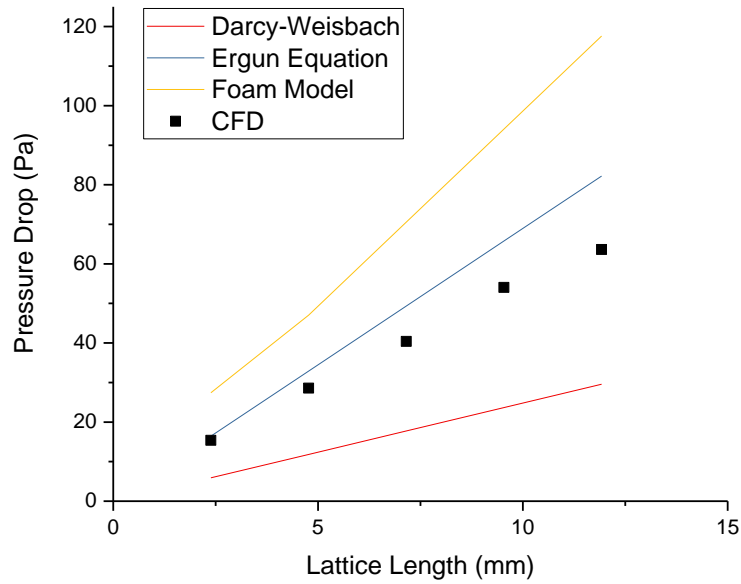


Figure 22: Pressure drop for Kelvin lattices comprised of 1-5 unit cells in the axial direction. Model fits for the Darcy-Weisbach, Ergun Equation, and Foam models are included.

Table 9: RMSE values for model fits of Kelvin lattice simulations.

	RMSE for Pressure Drop $\Delta P$ (Pa)
<b>Model</b>	$V_{superficial} = 2.2 \text{ m/s}$
<i>Darcy-Weisbach</i>	18.2
<i>Ergun Equation</i>	8.04
<i>Foam Model</i>	25.6

Figure 22 shows that the Ergun Equation offers the best model fit over the length of the lattice. From Table 9, we see that the RMSE value shows that the Ergun Equation predicts pressure drop within about 8.0 Pa on average. The and Darcy-Weisbach model underestimates

the pressure drop for all of the lattice designs, while the foam model overestimates the pressure drop for the lattice designs.

Next, the pressure drop after the Nth unit cell was determined in order to determine if changing the lattice configuration changes the pressure drop profiles. Again, as described in Chapter 3.3.1, determining if pressure drop is decoupled across lattice structures allows us to potentially use data-driven optimization without accounting for an interaction term that accounts for the position-induced pressure drop. Figure 23 below shows the pressure drop after the Nth unit cell for all lattice designs.

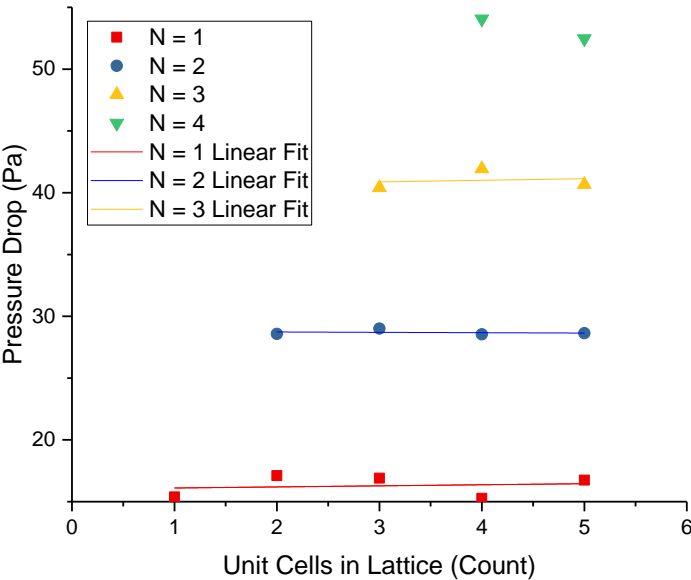


Figure 23: Flow decoupling after Nth unit cell for Kelvin lattice stack. ANOVA tested statistical difference between regression slopes and 0. N = 1 p-value = 0.802. N = 2 p-value = 0.828. N = 3 p-value = 0.802.

Figure 23 shows that pressure is quantitatively decoupled over Kelvin lattice structures with up to 5 unit cells in the axial direction for the flow condition of inlet flow velocity of 2 m/s. Each series in Figure 23 represent pressure drop after the corresponding unit cell ( $N=1$ ,  $N=1$ , ...). For pressure drop after the first, second, and third unit cells, a linear regression was performed in OriginLab. Regression could not be performed for pressure drop after the fourth and fifth unit cells, since lattices were only tested up to 5 unit cells in axial direction. The slope of the linear regressions were compared to 0 using an ANOVA test as described in Chapter 2.2.4. For all three of the regressions performed, the slopes were not statistically different from 0, with p-values for significance of  $p = 0.802$ ,  $0.828$ , and  $0.802$  for pressure drop after the first, second, and third unit cells, respectively.

These results importantly suggest that, at least for Kelvin unit cells of this geometry, pressure drop is at least decoupled under this flow condition up to the fourth unit cell. This is a vital conclusion that allows for the integration of these lattice structures into a data-driven optimization workflow.



## Chapter 4

### CONCLUSIONS AND FUTURE PLANS

#### 4.1 Conclusions

This project provides an investigation into fundamental fluid flow phenomena through unit cells and lattice structures with varied geometry and flow conditions. While this project has merely scratched the surface of this rich new intellectual well, there are important conclusion this work has discovered that can contribute to the body of understanding in lattice design, unit cell flow dynamics, theoretical model fits, and the potential to apply optimization techniques and automated workflows to design a lattice structure with desired flow dynamics.

##### 4.1.1 Flow Phenomena

Overall, investigating the qualitative fluid flow phenomena trends show that flow profiles develop through unit cells in predictable ways. Velocity profiles show that fluid velocity in the axial direction experiences a “flow conditioning” effect, where velocity increases through the pores of unit cells. Additionally, transverse velocity is predictably induced as flow approaches struts. The predictability and control offered by fluid flow phenomena highlight the promise order lattice structures offer to develop processes with highly controlled mass and heat transfer . Since traditional porous foams are disordered and stochastic, tuning the microstructure is difficult, so mass micro- and meso- scale flow phenomena are also stochastic. Here, we have shown that we can influence flow phenomena in predictable ways, which could be useful in many mass and transfer applications.

The relationship of individual unit cell geometry and flow conditions on pressure drop was also investigated in-depth for cubic unit cells. It was observed that pressure drop was somewhat difficult to predict with the state-of-the-art theoretical correlations. While icPOCS

was developed specifically for cubic geometries, the range of volume porosities, superficial velocities, and total lattice lengths over which the model accurately predicts pressure drop appears somewhat limited. Specifically for single unit cells, the model seemed to fit the best for superficial velocities below 5 m/s and volume porosities above 0.9. For future applications of using correlations to predict pressure drop over small number of unit cells, we recommend only using icPOCS under those specific circumstances. The accuracy of the Darcy-Weisbach model in predicting pressure drop came at somewhat of a surprise, but the model was generally the most accurate correlation, while the Ergun Equation consistently overestimated pressure drop. Ultimately, the observed model fits do motivate the need for better a better physics-based correlation that is more adaptable to a diverse range of unit cell geometries and flow conditions. Volume porosity was shown to be a reasonably good linear predictor of pressure drop, particularly for porosity values above 0.9. While this does not replace the need for a robust correlation, it is useful as a predictive tool to leverage volume porosity as a pressure drop predictor.

Pressure drop was shown to be quantitatively decoupled for cubic and kelvin lattices up to the fourth unit cell for flow conditions tested. Pressure drop after the Nth unit cell was shown to statistically stay constant, even when increasing the number of unit cells in the axial direction of the lattice. While this is a limited conclusion, it is an important first step in determining the feasibility of the optimization of lattice designs. Understanding that the pressure drop contribution of an individual unit cell is positionally-independent under specific conditions is vital towards implementing an optimization algorithm. It will be important moving forward to expand the bounds of the pressure decoupling. For example, knowing for how many unit cells is pressure still decoupled from position, or over what flow conditions, is important to increase the applicability of any optimization workflow.

## **4.2 Future Work**

The results of this project provide ample opportunities for future work, particularly in applying the validated CFD workflows towards optimizing a lattice assembly to exhibit desired flow dynamics. A portable optimization workflow is proposed and described below, for which a future researcher can implement.

### **4.2.1 Optimization of pressure drop through lattice structures**

The workflow is developed for an objective function with the goal of maximizing total lattice surface area, while minimizing pressure drop across the lattice length. This objective function is most relevant for an application in catalysis, where maximizing surface area is important for increasing the catalytic efficiency and ultimately reaction rate. This objective function is also relevant for an application for using lattice structures as particle collectors or for other transport-mediated applications, where surface area is an important factor in the efficiency of transport phenomena. Pressure drop functions as a surrogate for operating efficiency, since maintaining an operating pressure is important for flow to be realized in these applications.

#### **4.2.1.1 Workflow for optimization of lattice design**

The flow coupling experiments described in Chapter 3 concluded that, for Laminar flow conditions, pressure drop was decoupled for lattice assemblies of Kelvin and cubic unit cells of the same unit cell type. Thus, the first-pass optimization implementation will be limited to developing an optimized lattice structure that consists of unit cells of a fixed type (cubic or Kelvin) and cell length. The design parameters remaining to be manipulated are window size (or strut size), Laminar flow condition, and lattice configuration in 3-dimensional space (number in the X, Y, and Z directions).

Several inputted constraints are also needed to guide the optimization algorithm. The total length and width of the lattice must be fixed inside a pre-determined range, which would be dependent on the residence time needed for the catalytic application. For example, for a meso-scale reactor application, a length between 30-50 mm was used in the reactor design.<sup>21</sup> For the sake of this first-pass optimization, this same length range would be utilized for both the length, width, and height. Additionally, the minimum solid surface area needed to achieve desired catalytic kinetics would need to be inputted as a constraint as well. For a meso-scale reactor, a minimum surface area constraint of 500 mm<sup>2</sup> is reasonable based on literature values for meso-scale reactors.<sup>21</sup> Finally, since the cell length of the unit cells must be fixed, a cell length would be selected to match the radius of literature meso-scale reactors: 5 mm would be inputted as the set cell length.<sup>21</sup>

After the constraints of the design space have been implemented, a script would be generated to iteratively produce lattice CAD designs with varied window cell length and 3-dimensional configuration. This design automation would be implemented by scripting in the a command prompt environment, which is a platform that has been implemented for CAD designs in other applications.<sup>22</sup> To generate enough lattice structures in order to generate a large enough dataset for optimization, unit cell window sizes would be incremented by 0.05 mm from the minimum window size achievable (without closing the pore) for a cubic/Kelvin cell length of 5 mm, to the maximum printable window size that is achievable. The bounds for the minimum and maximum allowable window sizes as a function of unit cell type and cell length have been experimentally determined in the Fromen Research Group. The 3-dimensional lattice configuration designs will also be varied so long as the configuration stays within the length, width, and height constraints. Thus, the design of a sufficiently large number of lattice designs would be available for CFD simulations.

The validated CFD workflow described in Chapter 2 will then be applied to the lattice structures designed in order to generate pressure drop data over the length of the lattices. Analogously to the automated workflow described for generating lattice designs, a script will be developed to import a CAD file into SimScale and run the CFD workflow for a range of Laminar flow conditions. The script would set the flow inlet boundary condition based on the predetermined range of Laminar flow conditions. For example, flow could be simulated for  $Re_{window} \in [1, 1000]$ , incrementing the  $Re_{window}$  by 1. The script would recalculate the inlet flow velocity based on the unit cell geometry for the desired  $Re_{window}$ . The pressure drop data over the length of the lattice would be pulled from the CFD post-processor into a structured dataset.

Different multivariate regression models would then be tested on the dataset to develop a surrogate model,  $f(x)$ , that relates the influence of window size, 3-dimensional configuration, and flow condition, on the responses of pressure drop ( $y_1$ ) and surface area ( $y_2$ ). The options for multivariate regression models include simple multivariate linear, random forest, regularized linear, and principle component regression. While each of these approaches has inherent advantages and limitations for different types of datasets, it is difficult to predict which regression technique would offer the highest fidelity *a priori*. Thus, each of these regression techniques will be implemented in order to develop an array of surrogate models which can be analyzed to determine the model with the highest fidelity. Since the objective function is multi-objective, with 2 responses, a pareto plot will be developed to show the pareto front, the upper limit of surface area for minimized pressure drop. Finally, depending on an ultimate application, weights can be assigned to each of these responses, to determine ultimately which designs and operating conditions provide the optimal responses. Figure 24 below summarizes this workflow in a schematic.

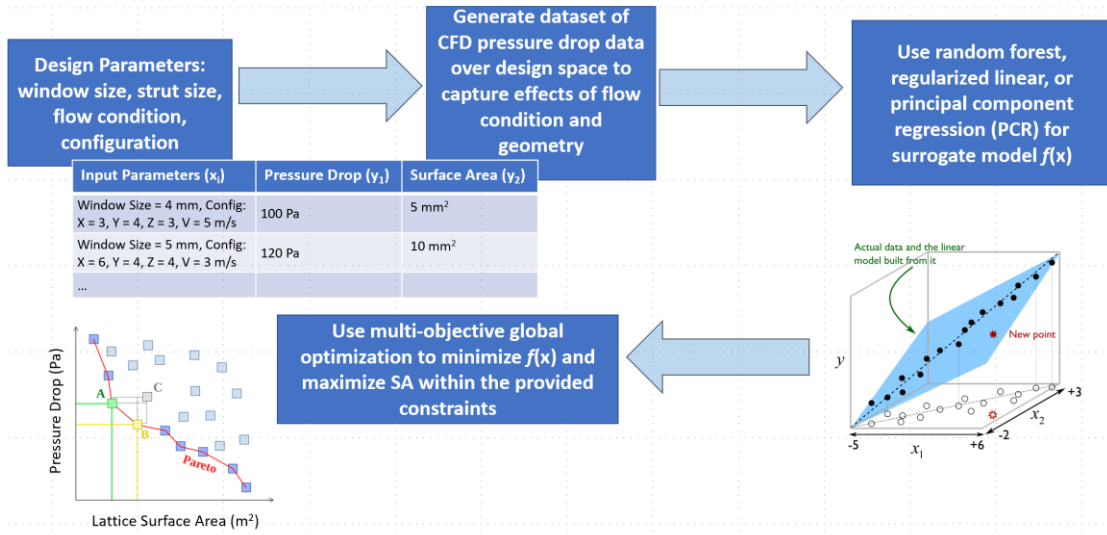


Figure 24: Schematic of optimization workflow

## REFERENCES

1. Nagesha, B. K., Dhinakaran, V., Shree, M. V., Kumar, K. M., Chalawadi, D., & Sathish, T. (2020). Review on characterization and impacts of the lattice structure in additive manufacturing. *Materials Today: Proceedings*, 21, 916-919.
2. Bartolo, P. J. (2011). *Innovative Developments in Virtual and Physical Prototyping: Proceedings of the 5th International Conference on Advanced Research in Virtual and Rapid Prototyping*, Leiria, Portugal, 28 September-1 October, 2011. CRC Press.
3. Klumpp, M., Inayat, A., Schwerdtfeger, J., Körner, C., Singer, R. F., Freund, H., & Schwieger, W. (2014). Periodic open cellular structures with ideal cubic cell geometry: Effect of porosity and cell orientation on pressure drop behavior. *Chemical Engineering Journal*, 242, 364-378.
4. Inayat, A., Klumpp, M., Lämmermann, M., Freund, H., & Schwieger, W. (2016). Development of a new pressure drop correlation for open-cell foams based completely on theoretical grounds: Taking into account strut shape and geometric tortuosity. *Chemical Engineering Journal*, 287, 704-719.
5. Maconachie, T., Leary, M., Lozanovski, B., Zhang, X., Qian, M., Faruque, O., & Brandt, M. (2019). SLM lattice structures: Properties, performance, applications and challenges. *Materials & Design*, 108137.
6. Inayat, A., Schwerdtfeger, J., Freund, H., Körner, C., Singer, R. F., & Schwieger, W. (2011). Periodic open-cell foams: pressure drop measurements and modeling of an ideal tetrakaidecahedra packing. *Chemical engineering science*, 66(12), 2758-2763.
7. Singh, S. P., Shukla, M., & Srivastava, R. K. (2018). Lattice modeling and CFD simulation for prediction of permeability in porous scaffolds. *Materials Today: Proceedings*, 5(9), 18879-18886.
8. Bracconi, M., Ambrosetti, M., Okafor, O., Sans, V., Zhang, X., Ou, X., ... & Tronconi, E. (2019). Investigation of pressure drop in 3D replicated open-cell foams: Coupling CFD with experimental data on additively manufactured foams. *Chemical Engineering Journal*, 377, 120123.
9. Das, S., Sneijders, S., Deen, N. G., & Kuipers, J. A. M. (2018). Drag and heat transfer closures for realistic numerically generated random open-cell solid foams using an immersed boundary method. *Chemical Engineering Science*, 183, 260-274.

10. Pan, C., Han, Y., & Lu, J. (2020). Design and Optimization of Lattice Structures: A Review. *Applied Sciences*, 10(18), 6374.
11. Wang, Y., Zhang, L., Daynes, S., Zhang, H., Feih, S., & Wang, M. Y. (2018). Design of graded lattice structure with optimized mesostructures for additive manufacturing. *Materials & Design*, 142, 114-123.
12. Daicong Da, Julien Yvonnet, Liang Xia, Minh Vuong Le, Guangyao Li. Topology optimization of periodic lattice structures taking into account strain gradient. *Computers and Structures*, Elsevier, 2018, 210, pp.28-40. [ff10.1016/j.compstruc.2018.09.003](https://doi.org/10.1016/j.compstruc.2018.09.003)ff. [ffhal-02265329f](https://doi.org/10.1016/j.compstruc.2018.09.003)
13. Abate, K. M., Nazir, A., Yeh, Y. P., Chen, J. E., & Jeng, J. Y. (2020). Design, optimization, and validation of mechanical properties of different cellular structures for biomedical application. *The International Journal of Advanced Manufacturing Technology*, 106(3), 1253-1265.
14. Autodesk Inc (2021). Fusion 360 (Version 2.0.10148). [Student License].
15. SimScale GmbH (2021). SimScale Computational Fluid Dynamics. [Student License].
16. Khan, M. M. K., & Hassan, N. M. (Eds.). (2015). *Thermofluid Modeling for Energy Efficiency Applications*. Academic Press.
17. OriginLab Corporation (2017). Origin(Academic) (Version 2017). [Academic License].
18. Deshmukh, S. R., & Vlachos, D. G. (2005). Novel micromixers driven by flow instabilities: Application to post-reactors. *AIChE journal*, 51(12), 3193-3204.
19. Rajani, B. N., Kandasamy, A., & Majumdar, S. (2009). Numerical simulation of laminar flow past a circular cylinder. *Applied Mathematical Modelling*, 33(3), 1228-1247.
20. Seo, I. W., & Song, C. G. (2012). Numerical simulation of laminar flow past a circular cylinder with slip conditions. *International Journal for Numerical Methods in Fluids*, 68(12), 1538-1560.
21. Styring, P., & Parracho, A. I. (2009). From discovery to production: Scale-out of continuous flow meso reactors. *Beilstein journal of organic chemistry*, 5(1), 29.



22. Moreno, R., & Bazan, A. M. (2017, October). Design automation using script languages. High-level CAD templates in non-parametric programs. In IOP conference series: materials science and engineering (Vol. 245, No. 6, p. 062039). IOP Publishing.